

ScholarWorks@GSU

Direct transfer techniques of graphene

Authors	Okmi, Aisha
Citation	Okmi, Aisha. "Direct transfer techniques of graphene." 2022. Dissertation, Georgia State University. https://doi.org/10.57709/32496116
DOI	https://doi.org/10.57709/32496116
Download date	2026-06-06 20:01:19
Link to Item	https://hdl.handle.net/20.500.14694/12295

Direct transfer techniques of graphene

by

Aisha Okmi

Under the Direction of Sidong Lei, PhD

A Dissertation Submitted in Partial Fulfillment of the Requirements for the Degree of

Doctor of Philosophy

in the College of Arts and Sciences

Georgia State University

2022

ABSTRACT

This thesis mainly focuses on the direct transfer techniques of CVD graphene. Two new methods to transfer graphene with no severe contamination have been reported. The effect of surface tension has been investigated experimentally. Based on several experiments to study the effect of surface tension on graphene transfer, we designed a method in which there is no need to reduce the surface tension of water. This conventional method was employed to achieve a whole device transfer in only one step. In addition, we proved that surface tension can be an essential factor in creating a graphene/water membrane that is functioned to transfer graphene to any type of substrate. This composite membrane turns out to be the most effective way to widen graphene applications. We found that liquid media with surface tension lower than that in water cannot be functioned to achieve this type of transfer. Briefly, graphene/ water membranes at high surface tension can be peeled from water with PET film assistance. Using this method, we transfer graphene to rigid and stretchable substrates, which guarantees this method is a promising technique for widening graphene usage in biomedical and environmental applications. Although the two processes, conventional and graphene/ water membrane, are utilized to transfer graphene to several materials with no severe contamination, the graphene/water composition method effectively processes the flattest graphene.

INDEX WORDS: Surface tension, Graphene, Polymer-free transfer, Water-IPA mixture, Surface tension gap, CVD growth, Graphene/water membrane

Copyright by
Aisha Okmi
2022

Direct transfer techniques of graphene

by

Aisha Okmi

Committee Chair: Sidong Lei

Committee: Vadym M Apalkov

Mukesh Dhamala

Electronic Version Approved:

Office of Graduate Services

College of Arts and Sciences

Georgia State University

December 2022

DEDICATION

For Ghadi, Laian, Lama, Aseel, Rafa, Rafeef, Mayar, Ahmed, Khalid, Ali, Mo'aiad,
Mohammed, Eyad, and Battal.

ACKNOWLEDGEMENTS

I am most grateful to my advisor and the chair of my Ph.D. committee Dr. Sidong Lei for his patient guidance, constant support, and opportunities. Working in his group was indeed a wonderful experience filled with exciting experiments and inspirational discussions.

I also want to thank Dr. Mukesh Dhamala and Dr. Vadym Apalkov, my committee members, for their time and helpful comments on my dissertation evaluation.

Very special thanks to the graduate director of the physics department at Georgia state university, Dr. Murad Sarsour, for his guidance and support in all my Ph.D. studies.

I want to thank Dr. Xiaochun He, the previous graduate students' director at the physics department, for guiding me through my application processes for my Ph.D. admission.

Part of the experiment reported in this dissertation was done in CNMS, ORNL, under the guidance of Dr. Kai Xiao and Dr. Ivan Vlassiuk. Thanks to them for giving me the space and materials to achieve the needed experiments.

Thanks Dr. Guanhui Gao, Rice university, for achieving the TEM measurement reported in the third chapter.

Thanks Dr. Ondrej Dyck, CNMS, ORNL, for achieving the TEM measurements reported in the second and fourth chapters.

Thanks to Dr. Boxing Xu, and Dr. Xuemei Xia, and Yue Zhang, the University of Virginia, for doing the simulation section and establishing the theoretical model of the graphene/water membrane concept.

Thanks to Dr. Pei Dong and Dr. Rui He for doing the contact angle measurements in the fourth chapter.

Special thanks to my friends Rowuda Althagfi, Rezvan Husseini, Jawad Zafar, Aranyo Mitra, Chandrama Mukherji, Beena Meena, Olugbenga Olunloyo, Krishna Magar, Shimaa Almalki, Yahya Alhazmi, and Rasha Mashour, for believing in me always and supporting me in all hard times.

Thanks to my lovely aunt Maryam Ibrahim who supported my plans and believed in me.

Thanks to my wonderful parents, I would not be able to achieve anything without their support.

Thanks to my sisters and brothers, they always believe in me and support me.

Thanks to my lab mates, Ningxin Li, Tara Jabegu, and Diren Maraba, for their help and support.

TABLE OF CONTENTS

ACKNOWLEDGEMENTS	II
LIST OF TABLES	VII
LIST OF FIGURES	VIII
LIST OF ABBREVIATIONS	XIV
INTRODUCTION.....	1
Graphene features	1
The synthesis of graphene	1
The transfer techniques of graphene.....	2
1 CHAPTER 1: LARGE AREA GRAPHENE GROWTH.....	4
1.1 Chemical Vapor Deposition	4
<i>1.1.1 Pre-growth preparation processes</i>	<i>4</i>
<i>1.1.2 Low pressure chemical vapor deposition.....</i>	<i>6</i>
<i>1.1.3 Atmospheric pressure chemical vapor deposition</i>	<i>6</i>
1.2 After graphene growth:	7
<i>1.2.1 Plasma etching of the bottom graphene layer</i>	<i>7</i>
<i>1.2.2 Graphene on copper</i>	<i>8</i>
<i>1.2.3 Transfer graphene to the target substrate</i>	<i>9</i>
2 CHAPTER 2 GRAPHENE TRNASFER TECHNIQUES	11

2.1	Polymer-assistance graphene transfer	11
2.1.1	<i>Disadvantages of polymer-assistance transfer</i>	<i>13</i>
2.2	Polymer-free transfer.....	14
2.2.1	<i>Examples of polymer-free transfer techniques</i>	<i>14</i>
2.3	The effect of surface tension on graphene	16
2.4	Defective graphene	16
3	CHAPTER 3 A DIRECT SIMPLE METHOD TO TANSFER GRAPHENE	18
3.1	Experiments:.....	19
3.1.1	<i>Copper etching and Graphene Transfer.....</i>	<i>20</i>
3.1.2	<i>Surface Tension Tuning.....</i>	<i>22</i>
3.1.3	<i>Transfer Procedure</i>	<i>23</i>
3.2	Surface Tension Effect.....	25
3.3	Whole device transfer	29
4	CHAPTER 4: GRAPHENE WATER MEMBARENE	31
4.1	Experimental implementation of GWM	31
4.2	Theoretical modeling of GWM	36
4.3	GWM-enabled one-step graphene suspension with no polymer residues	40
4.4	GWM-enabled high-quality graphene transfer on substrates.....	42
	CONCLUSION	49
	REFERENCES.....	50

APPENDICES	55
Appendix A	55
<i>Appendix A.1.....</i>	<i>55</i>
<i>Appendix A.2.....</i>	<i>56</i>
<i>Appendix A.3.....</i>	<i>60</i>
<i>Appendix A.4.....</i>	<i>61</i>
Appendix B	62
<i>Appendix B.1.....</i>	<i>62</i>
<i>Appendix B.2.....</i>	<i>62</i>
<i>Appendix B.3.....</i>	<i>63</i>

LIST OF TABLES

Table 1 Surface tension values matching each IPA ratio	55
--	----

LIST OF FIGURES

Figure 1.1 Electropolishing of copper foil prepared for the growth. a) 25 mm × 50 mm, thickness is 25μm copper foil (unpolished). b) the copper piece after the electropolishing in phosphoric acid for 2 minutes.....	5
Figure 1.2 Homemade low pressure chemical vapor deposition LPCVD system for graphene growth. We used electropolished copper to grow graphene (shown the image on the left)6	6
Figure 1.3 a) Argon plasma etching setup. b) Plasma chamber during the etching that takes in 1 minute. c) The clamp designed to etch the graphene on the bottom copper side. d) The intact graphene facing down while the etched side facing up.	8
Figure 1.4 graphene on copper after 20 minutes LPCVD growth.	8
Figure 1.5 SEM images of graphene grown on copper 25 μm thickness using LPCVD (left and middle images) .On the right, graphene grown on copper film 75 μm thickness using APCVD.....	9
Figure 1.6 Atomic force microscopy AFM on the left. AFM image of graphene transferred on SiO ₂ /Si (in the middle). The arrows shows the grain binderies. On the right side, a microscopic image of graphene on SiO ₂ /Si., which scanned using AFM.	10
Figure 2.1 Schematic drawing of polymer- assisted transfer steps.....	12
Figure 2.2 a) Polymer-assistance graphene transferred on Si/SiO ₂ (inset). A microscopic image of the same graphene. b) free-standing graphene transferred on TEM grid using polymer support transfer method. c) Graphene transferred on Si/SiO ₂ , following the direct transfer method. d) Graphene transferred on TEM grid following the direct transfer method.....	13

- Figure 2.3 Isopropanol alcohol IPA was added to the etching solution (0.1 M of ammonium persulfate). 1:11 to reduce ST. We can see that IPA reduced the etching efficiency and led to highly copper contamination on graphene. 15
- Figure 2.4 a) Defective graphene on the right vs an intact graphene structure. b) Copper residues on top of graphene after the copper substrate etched away (left) on the right, graphene edge deformation edges result of O₂ leakage. c) defective graphene transferred using polymer on SiO₂. Graphene with copper residues transferred on SiO₂. d) Graphene/ SiO₂ with copper contamination. 17
- Figure 3.1. The transferring cell that designed to achieve the direct transfer of graphene including 2 sided syringes connected to the transfer reactor that made of Teflon. 21
- Figure 3.2 a) shows the reactor design. b) shows the reactor during the copper etching after connecting the both sided opening to the tubes. c) shows the retainer film that enclosed copper/ graphene during etching. d) schematic of graphene/copper piece enclosed by the retainer film. 21
- Figure 3.3 a) shows a graph of the IPA ratios and ST final values. b) Shows a graph of IPA ratios and surface tension gaps STGs. 23
- Figure 3.4 a) Graphene after replacing the etching solution with DI-water (ST 72 dyne/cm). b) graphene after applying series STGs to reach the minimum ST at 32 dyne/cm . c) A substrate had been inserted behind graphene after ST reduction to achieve the transfer. d) Graphene on 300nm SiO₂ substrate. e) Defective graphene on copper during copper etching. f) Defective graphene with edge deformations after the copper is fully etched (the original square shape changed to a star shape). 25

- Figure 3.5 a) Shows an image of graphene before applying STG higher than 40 dyne/cm. b) Shows an image of graphene that got a small shrink after applying STG higher than 40 dyne/cm. c) Graphene tore up after applying 46 dyne/cm STG. 27
- Figure 3.6 a) Raman shift of monolayer graphene transferred on 300nm SiO₂ after applying the maximum surface tension gap (40 dyne/cm). We can see that the 2D peak is almost double the G peak, which confirms that graphene is a monolayer. The inset image shows an AFM image of the same graphene with a roughness of 2.9 nm. b) TEM image of single-layer graphene transferred with pure DI-water. 29
- Figure 3.7 a) Device/Graphene/Cu during etching. b) Device/Graphene/Cu floating on the etching solution after copper is fully etched. c) After finalizing the transfer. d) Magnified image of the device/Graphene/SiO₂. 30
- Figure 4.1 a) Free-standing GWM held by a PET frame. b) Home-designed fixture for graphene plasma removal. Copper foil with CVD graphene grown on both sides is clamped on the fixture, with one side exposed to radio-frequency plasma, while the other side is electrically shielded by the cavity formed with the copper foil and the pocket on the metal fixture. The shielded copper side has no physical contact with the surroundings, ensuring the graphene integrity. c) PTFE reactor with source and drain designed for copper etching and liquid replacement. 33
- Figure 4.2 .a) The copper foil is relocated into a specially designed reactor filled with 0.1 mol/L ammonium persulfate. b) Graphene floating on pure DI-water that inserted gradually to replace etchant. 34

- Figure 4.3 Free-floating graphene before and after liquids exchange: On the left, graphene floating on 0.1M of ammonium persulfate. On the right, graphene floats on pure DI water..... 35
- Figure 4.4 Several defects (edges deformation, shrinking, and visible holes) can be developed during the growth and jeopardize the graphene quality..... 35
- Figure 4.5 a) *Optical image of the graphene peeling process with a peeling angle of 54.6° when pure DI water is employed. b) Criteria of success peeling. The required minimum peeling angle increases and the liquid contact angle decreases (i.e., the liquid become more hydrophilic). When the configuration falls in the successful range, the graphene-water membrane can readily form and be isolated from the liquid surface. If in the failure zone, the membrane breaks. Inset: the definition of peeling angle. c) Contact angle measurement of water on a graphene surface. d) Molecular dynamics simulation of the graphene peeling process. The figures illustrate the frames of the dynamics at 0, 3.5, and 6 s after the peeling starts. The peeling angle is set at 57.5° to ensure a successful peeling in the simulation. e) Simulated evolution of the peeling force as a function of time and IPA concentration. f) A smaller contact angle (induced by higher IPA concentration) requires a larger peeling angle and thus, increases the surface area of the liquid membrane, increasing the risk of membrane breaking and peeling failure. 38*
- Figure 4.6 A successful peeling of GWM from a liquid contains 1% IPA to 99% DI water (left), and a liquid contains 2% IPA to 98% DI water (right)..... 40
- Figure 4.7 a) *STEM image of graphene transferred with GWM. The low-resolution image shows clean graphene surface, and the high-resolution image (inset) clearly distinguish carbon atoms. b) SEM image of free-suspended graphene directly produced by the GWM, and*

<i>the magnified image (inset) shows no contamination. c) Raman spectrum of the free-suspended graphene.</i>	41
Figure 4.8 MD simulation confirms that water molecules do not adhere to the graphene layer being peeled off.....	42
Figure 4.9 a) Graphene-wafer membrane for transfer. b) Raman spectrum of the as-transferred graphene. Inset: Optical image of the as-transferred graphene. c) AFM image of graphene transferred on Si/SiO ₂ wafer with graphene-water membrane. d) Conventional graphene transfer method with target-substrate merged into liquid. The liquid is drawn out of the reactor to lower graphene and laminate it onto the substrate. Because there is liquid trapped on the graphene-substrate interface, wrinkle develops after the liquid evaporates. e) AFM image of graphene transferred onto Si/SiO ₂ wafer with the conventional polymer-free procedure. f) Graphene transfer procedure with flipped graphene-water membrane to further eliminate water trapping on interfaces. g) AFM image of the flipping transfer with better flatness and transfer quality.	44
Figure 4.10 Field-effect transistors ((a) inset) had been fabricated with the same batch of graphene layers transferred with the conventional and our newly developed polymer-free transfer approach. The FET made with the conventional polymer-free method (a) yields mobility of 380 cm ² V ⁻¹ s ⁻¹ , whereas our new method renders a significant improvement up to 700 cm ² V ⁻¹ s ⁻¹ as shown in (b).	46
Figure 4.11 (a Graphene-water membrane transfer onto a hydrophobic substrate with the assistant of a hydrophilic frame. b) The hydrophilic frame holds the water and retains the tension that flattens the graphene layer until the graphene layer is laminated firmly onto the substrate. c) Optical image of graphene transferred onto silicon with SiO ₂ frame	

severing as a hydrophilic frame. d) AFM image of as-transferred graphene on the silicon surface shown in (c). e) Graphene layer transferred on the hydrogel. (1 g of agar and 0.2 g gelatin dissolved in 100 ml DI water). 47

LIST OF ABBREVIATIONS

Chemical vapor deposition (CVD)

Graphene oxide (GO)

Grain boundaries (GB)

Low pressure chemical vapor deposition (LPCVD)

Atmospheric pressure chemical vapor deposition (APCVD)

Poly(methyl methacrylate) (PMMA)

Graphene water membrane (GWM)

Isopropanol alcohol (IPA)

Scanning Electron Microscopy (SEM)

Root mean square (RMS)

Atomic force microscopy (AFM)

Polydimethylsiloxane (PDMS)

Scanning Transmission Electron Microscopy (STEM)

Surface Tension (ST)

Surface Tension Gap (STG)

Polytetrafluoroethylene (PTFE)

Polyethylene Terephthalate (PET)

INTRODUCTION

Graphene features

Since carbon thin films (graphene) first exfoliated successfully in 2004 [1], more efforts have been devoted to exploring the remarkable features of this material. Intrinsic graphene that can be exfoliated from graphite has 0.331 nm thickness, is thermally conductive, and has very high electron mobility reaching $10000 \text{ cm}^2/\text{V}\cdot\text{s}$. [1]. Graphene is classified as one of the most mechanically robust materials; that property is attributed to the strong sp^2 hybridized bonds in graphene [2]. This only-one-atom thickness transparent, strong sheet is one of the best choices for many applications in the field of materials lamination and the fabrication of solar cells [3]. In addition, the transparency and the very high electron mobility also nominate graphene as a spectacular material for electrodes fabrication [4]. The microscale peeled graphene contributed to several studies that reveal the remarkable features of those materials, such as the Quantum Hall Effect (QHE) at room temperature [5], making it one of the distinctive low dimensional materials to study QHE phenomena. In surface studies, graphene provides fascinating findings related to the nature of this material and how it interacts with gases, metallic surfaces, and liquids [6-9]. The simple reduction of graphene to graphene oxide (GO) by introducing defects and the easily reversible process create more exciting studies and applications in graphene-based materials [6, 10]. Although all this distinctive features of graphene, peeled microscale graphene is inadequate for most desirable studies and applications. Consequently, the need to produce large graphene sheets artificially was an ultimate need.

The synthesis of graphene

As mentioned before, exfoliated graphene is unscalable, which is undeniably restriction in most graphene studies and applications. The need for large-scale graphene led to several

techniques to synthesize graphene that would reach meter square to fulfil technical and commercial demands. Epitaxial growth techniques have been highly functioned to generate relatively large graphene film [11-15]. One of the first methods to grow a few centimeters of graphene was reported in 2009 [11]. Graphene that was produced by chemical vapor deposition (CVD) on copper and transferred to SiO₂/Si with polymer assistance [11], [16], recorded electron mobility slightly less than half of the mobility that was recorded on intrinsic graphene. The unavoidable defects, such as grain boundaries (GB) that would produce as a result of the growth dynamics and inevitable contamination that the transfer substances would generate, could lead to a remarkable reduction of the final quality of the graphene that is synthesized following the chemical vapor deposition. The efforts to improve the quality of graphene produced by using epitaxial growth techniques, especially CVD, have grown since the first successful growth in 2009. Three types of graphene growth have been reported since 2009. The first chapter of this dissertation will briefly show low-pressure chemical vapor deposition (LPCVD), which is the method followed to grow the graphene to achieve the target study of this dissertation. Oppositely, atmospheric pressure chemical vapor deposition (APCVD), which produces graphene with very high quality and less technical setup, will also be discussed in the same chapter.

The transfer techniques of graphene

Since synthesized graphene is usually grown on metallic substrates such as copper or nickel; however, achieving characterization and related electric and mechanical measurements requires graphene to be transferred to another type of substrates such as Si or SiO₂. Processes, including etching the metallic substrate, removing the etchant solution and, rinsing graphene, then finally transporting it to another specific substrate, are called transfer [11, 16]. Although the transfer of 2D materials is a large topic, it can be classified into two types. The first type is polymer-

assistance transfer. In this type, graphene on the etchable metallic material would be coated with a polymer, for example, Poly(methyl methacrylate) (PMMA) [11, 16]. Even though polymer assist transfer is simple and can guarantee the success of the whole transfer steps, it would produce highly contaminated graphene. This fact led to tremendous efforts to design methods that would contribute to the direct transfer of graphene to the target substrate [17]. This dissertation will detail studies about the direct transfer of graphene. First, I will show the lab capability in the graphene growth matter which include CVD growth process and plasma etching that were applied on the graphene that is used to achieve all the required experiments. Later, I will give a short introduction to some current transfer techniques. In the third chapter, I will show the first method was designed based on surface tension calculations, such as the maximum surface tension that can be applied to graphene during the transfer [18]. Finally, the concept of the graphene water membrane (GWM) will be introduced. We found that graphene can be peeled from the water surface, and this new peeling process would lead to the design of a new method to transfer graphene into any material. [19]. The fourth chapter of this dissertation will show experimental results, theoretical calculations, and molecular dynamics simulation of the peeling of GWM. The experimental and molecular dynamics simulation models confirm that the high surface tension of water is an essential factor in succeeding in graphene transfer.

1 CHAPTER 1: LARGE AREA GRAPHENE GROWTH

All graphene that we employed to establish the direct transfer techniques and to study the impact of surface tension on those techniques and the related applications was grown using a homemade chemical vapor deposition CVD system. In general, we achieved the growth at a high temperature of around 1000° C. Copper foil was used as a metallic catalyst. Gases, including H₂:Ar (1:9) and methane CH₄, were utilized as precursors. To guarantee that the graphene we are functioning in our research is monolayer, we used O₂ and Ar plasma to etch the graphene layer that grew on the copper foil bottom side. In this chapter, I present low-pressure chemical vapor deposition LPCVD and atmospheric pressure chemical vapor deposition APCVD and all the related processes to guarantee the quality of monolayer graphene.

1.1 Chemical Vapor Deposition

1.1.1 Pre-growth preparation processes

Chemical electropolishing: Chemical treatment plays an essential role in improving the final graphene quality; specifically enhancing graphene coverage [20]. We dissolved 0.5g of urea in 10 ml of deionized water that we mixed later with 90 ml of 85% phosphoric acid. A surfactant was employed to smooth the bubbles on the copper surface and improve the electropolishing process. The copper used for the graphene growth has a thickness is 25µm. Six Volts were applied on a 25 mm × 50 mm copper piece for 4 minutes; the produced current through the electrolyte was 1.5 A. After electropolishing, the copper was immersed in DI water, then Isopropanol alcohol (IPA). Next, we used an Ar gun to dry it before inserting it into the CVD quartz tube. During the chemical treatment, namely the electropolishing, the target catalyst (copper foil) undergoes surface ions removal [21], the process that produces a smoother surface with less roughness and oxidation, as we can see in Figure 1.1. The original status of the copper would require more or less

pretreatment. For instance, an unpolished copper surface might need to either be etched using nitric acid or electropolishing in highly concentrated phosphoric acid for 30 minutes to remove the unavoidable oxidation and produce a uniform surface. Another essential advantage of chemical treatment is copper cleansing, which reduces the contamination that would be adhered to the copper during the original finishing. Figure 1.1 shows the oxidation on the sides of copper film reduced after electropolishing for 2 minutes.

Leakage test: Before achieving the growth, specifically low-pressure graphene growth, we purge the system with Ar and H₂ for 1 hour. Then, we pump the system down for another hour. Finally, we stopped the pumping down and then counted for 30 minutes to check the leakage. In most of the cases where slight leakage had been recorded, we do the helium leakage test. Air (O₂) leakage to the growth chamber would severely affect the growth and the graphene's final quality, as stated in the next chapter.

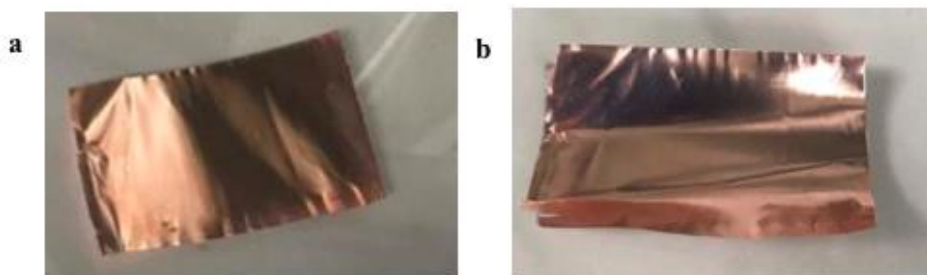


Figure 1.1 Electropolishing of copper foil prepared for the growth. a) 25 mm × 50 mm, thickness is 25 μm copper foil (unpolished). b) the copper piece after the electropolishing in phosphoric acid for 2 minutes.

1.1.2 Low pressure chemical vapor deposition

After achieving the leakage test, we ramped the temperature to 1000° C in one hour. Copper was annealed for 30 min in a gas mixture of Ar and H₂ (90% :10%) 6 sccm. The growth was achieved at the same temperature with CH₄ flowrate is 35 sccm for 20 minutes. During this type of growth, we maintain the pressure inside the tube growth to 100 mT during annealing and 500 mT during the graphene growth. Figure 2.1 shows the LPCVD system used for this goal. Before starting the growing graphene process, we tested the leakage. As is shown in the pressure gauge, the vacuum level was held for 20 min, indicating no air leakage, which can guarantee the coverage of the graphene film. Scanning electron microscopy (SEM) of graphene grown using this method is shown in Figure1.5.

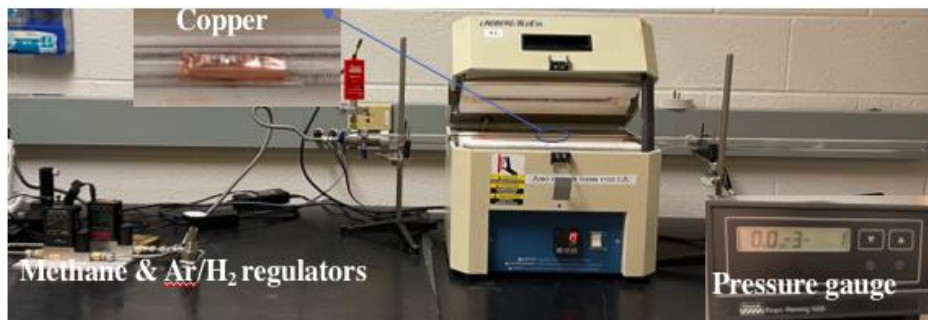


Figure 1.2 Homemade low pressure chemical vapor deposition LPCVD system for graphene growth. We used electropolished copper to grow graphene (shown the image on the left)

1.1.3 Atmospheric pressure chemical vapor deposition

Unlike the LPCVD, APCVD functions for the growth of graphene film at atmospheric pressure [22]. In this method, precursor gases will be inserted into the growth chamber at flow rates much higher than that in the LPCVD to reach pressure inside quartz equal to the outside. However, both methods produce continuous large graphene films at high temperatures, using the

same gas precursors and the metallic catalyst such as copper and nickel. SEM images of graphene grown using this method is shown in Figure 1.5.

1.2 After graphene growth:

1.2.1 Plasma etching of the bottom graphene layer

Graphene grown following the CVD techniques will be deposited on both sides of the copper film. However, the graphene layer grown on the bottom side is of lower quality because it is not a continuous film and is mostly not a uniform monolayer. In this matter, O₂ plasma will be functioned to remove the bottom graphene layer. Although O₂ plasma etching is very effective in removing the undesired graphene on the copper bottom side, we switched to radiofrequency Ar plasma which would reduce the risk of producing O₃ that might affect the intact graphene layer on the top of copper film. To achieve this most safely, we design a special mount holder with a specific clamp that makes it easy to apply the Faraday cage to protect only one side of grown graphene. The setup for the plasma etching process is shown in Figure 1.3.

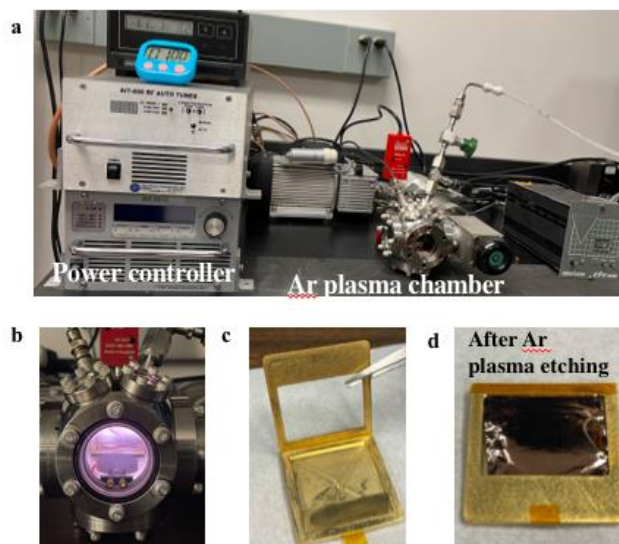


Figure 1.3 a) Argon plasma etching setup. b) Plasma chamber during the etching that takes in 1 minute. c) The clamp designed to etch the graphene on the bottom copper side. d) The intact graphene facing down while the etched side facing up.

1.2.2 Graphene on copper

After the CVD growth, a single layer of graphene is deposited on copper film, as shown in Figure 1.4. Although it is evident that monolayer graphene on copper is undistinguishable, SEM images can confirm the graphene coverage. SEM images of graphene grown on copper achieved using LPCVD and APCVD can be seen in Figure 1.5.



Figure 1.4 graphene on copper after 20 minutes LPCVD growth.

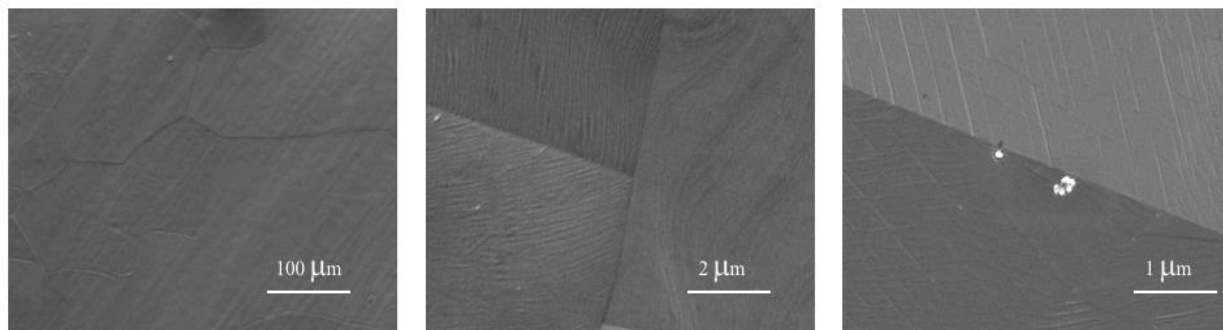


Figure 1.5 SEM images of graphene grown on copper 25 μm thickness using LPCVD (left and middle images). On the right, graphene grown on copper film 75 μm thickness using APCVD.

1.2.3 Transfer graphene to the target substrate

Transferring graphene to another substrate is the most crucial step after the growth since it is the keyword for further characterization, measurements, and applications. For example, a precise root mean square (RMS) roughness measurement of graphene can be achieved after transferring graphene on SiO_2/Si wafer using Atomic force microscopy (AFM), as shown in Figure 1.6 image on the left and middle. After transferring graphene, we made a scratch on a very small area of the SiO_2 , as shown in Figure 1.6. (right image). The image in the middle of Figure 1.6 shows the graphene coverage and the grain boundaries GB. The following chapters will show detailed techniques to achieve this step. It is worth mentioning that graphene transferred using the conventional direct transfer (unannealed) in Figure 1.6 has a RMS roughness of 4 nm.

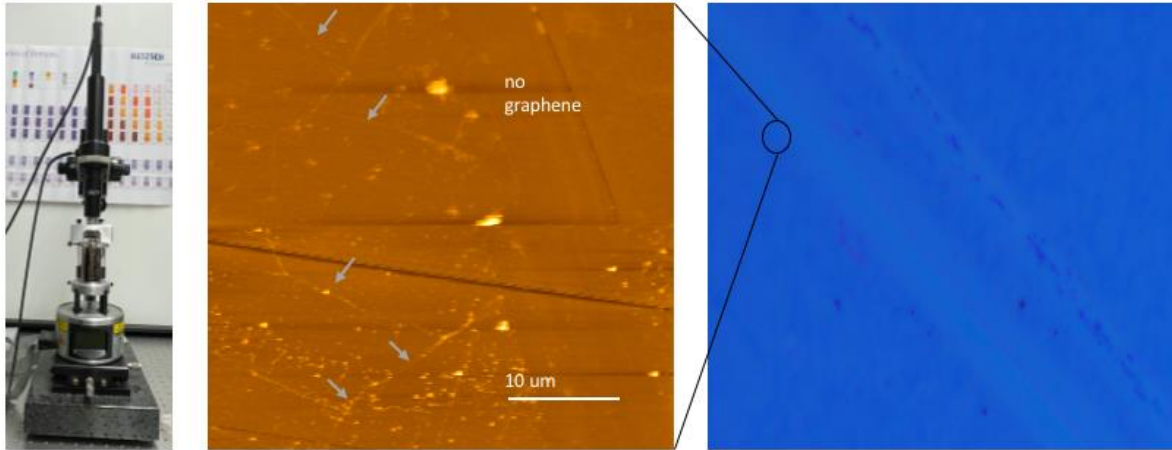


Figure 1.6 Atomic force microscopy AFM on the left. AFM image of graphene transferred on SiO₂/Si (in the middle). The arrows shows the grain binderies. On the right side, a microscopic image of graphene on SiO₂/Si., which scanned using AFM.

2 CHAPTER 2 GRAPHENE TRANSFER TECHNIQUES

Graphene grown on copper using CVD methods requests further processes to etch copper and transfer graphene to other types of substrates, such as Si or Si/SiO₂ or glass. For this purpose, researchers in the field of graphene synthesis invented several methods to transfer graphene to rigid and flexible substrates in preparation for the next steps, such as characterization and device fabrication. In general, transfer techniques can be classified into two categories. The first class is polymer-assist transfer, which includes applying a thin layer of polymer on graphene/copper to provide surface support during the chemical etching of copper and the rinsing process. The second category is the polymer-free transfer method or the direct transfer technique, which includes either applying non-polymer materials on graphene, such as some types of wax (paraffin), or designing methods to reduce the effect of surface tension of water on graphene while metallic substrate etching and later processes. This chapter introduces the prominent reported work in the field of transfer techniques.

2.1 Polymer-assistance graphene transfer

A polymer such as Poly(methyl methacrylate) PMMA and Polydimethylsiloxane (PDMS) [11] contributed to one of the initially reported methods to transfer graphene to a wide class of the rigid substrates such as Si, SiO₂ wafers, glass, and sapphire. Polymer-assistance transfer is a prevalent method since it is simple, fast, and can guarantee the integrity of transferred graphene. In this type of transfer, PMMA will be applied and spin-coated on the Gr/Cu piece using any type of the commercially available spin coaters. The produced thin polymer layer on Gr/Cu can be in the range 100-500 nm. After coating, the Gr/Cu will be left in a glass container filled with a copper etchant such as ammonium persulfate (NH₄)₂S₂O₈ or iron fluoride FeCl₃ [11] for half an hour to fully etch the copper. Then, we employ the target substrate to scoop polymer film/graphene from

the etchant and move it to pure DI water to remove the etchant residues. An Ar gun will be used to dry graphene on the substrate. To remove the polymer, we leave the target substrate/Gr/polymer in an organic solvent such as acetone for 10 minutes to dissolve the polymer. Later, we move it immediately to isopropanol alcohol IPA. The steps of transferring graphene following polymer-assisted transfer are shown schematically in Figure 2.1. A microscopic image of graphene transferred using this way shown in Figure 2.2. At this step, we can measure the roughness of the transferred graphene using atomic force microscopy AFM. It also can be used to fabricate devices depending on its quality. We functioned this method to transfer graphene on both SiO₂/Si and several types of metallic mesh to achieve scanning transmission electron microscopy (STEM), as shown in Figure 2.2.

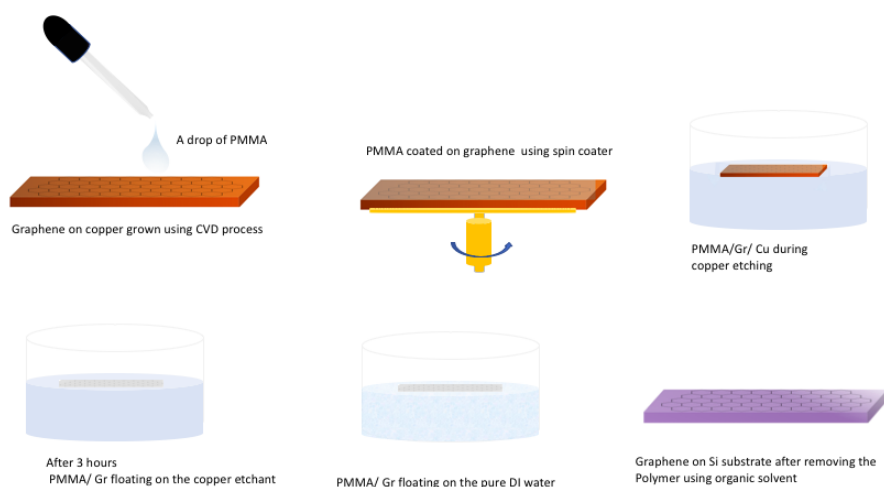


Figure 2.1 Schematic drawing of polymer- assisted transfer steps.

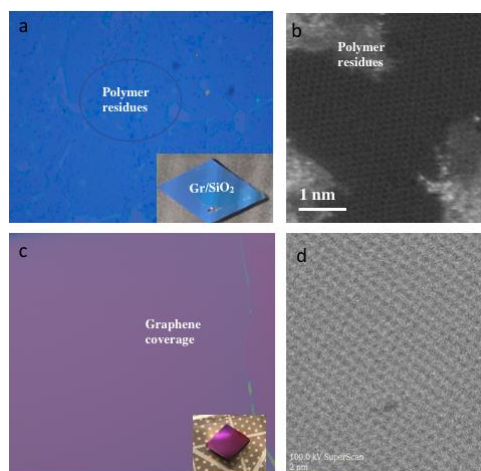


Figure 2.2 a) Polymer-assistance graphene transferred on Si/SiO₂ (inset). A microscopic image of the same graphene. b) free-standing graphene transferred on TEM grid using polymer support transfer method. c) Graphene transferred on Si/SiO₂, following the direct transfer method. d) Graphene transferred on TEM grid following the direct transfer method.

2.1.1 Disadvantages of polymer-assistance transfer

As mentioned above, polymer-assistance transfer is very effective in successfully transferring graphene. However, there are some common disadvantages to following this method. The first disadvantage of applying polymer is the limitation on the choices of target substrates; consequently, the graphene applications. Removing the polymer is a critical step; for this matter, soaking substrate/graphene/polymer in an organic solvent such as acetone for a few minutes is a requirement. However, flexible substrates, which can be deformed while immersing in an organic solvent, will be excluded for achieving this type of transfer. Consequently, a wide broad of graphene applications cannot be achieved by following polymer-assistance transfer. For example, most graphene-based pressure sensors applications require the graphene to be transferred on

stretchable materials that cannot be treated by acetone, which can cause major damage to their structure. The second issue related to this type of transfer is the produced contamination. Although soaking graphene with polymer in acetone at relatively high temperatures is an approved method to remove polymer, there are micro residues that will not be removed. This disadvantage produces the need for further annealing of the graphene at very high temperatures would reach 900° C in a vacuum to remove those inorganic particles. These harsh treatments would risk the final quality of the transferred graphene. The two main disadvantages stated above of this type of transfer produced the need to design other ways to make more effective results with less contamination, as detailed in the next section.

2.2 Polymer-free transfer

Isolating graphene from water to transfer it to the target substrate with no polymer coating is a challenging task. The prolonged belief in the water surface tension effect on graphene led to the design of complicated methods to achieve polymer-free graphene transfer. We can classify polymer-free transfer methods into two categories. The first class is the techniques in which polymer would be replaced by other non-polymer materials such as wax or a specific type of solid plastic thin film. The second category is achieving the transfer without surface assistance but with reduced surface tension.

2.2.1 Examples of polymer-free transfer techniques

One of the first reported techniques was the direct transfer of graphene on Au TEM grid with lacey carbon. 2009 [23]. Unlike the methods that showed up gradually after the success of growing large graphene sheets, this method depends on the effect of IPA surface tension and its evaporation to enhance the contact between the TEM grid and the transferred graphene. Reducing the water surface tension effect of copper etchant and DI water by mixing them with IPA at specific

ratios to achieve the transfer successfully was reported in 2014 [24]. This method contributed to the relatively large graphene transfer area in the range of centimeters. However, following this manner leads to prolong the etching time for few hours; consequently, not very effective metallic etching as shown in Figure 2.3., copper was not fully etched after transferring graphene. Hexane, an organic chemical, was functioned too to trap graphene in a lower surface tension interface to achieve clean transfer of graphene [25]. The principle of this method is to achieve the graphene transfer by providing surface support to graphene during copper etching and the transfer process. Another material that is applied to provide surface support to graphene and eliminate the possible effect of surface tension is paraffine [26]. In addition to the previous methods, lamination is a common way to transfer graphene. Following this way, materials in sheet shape with a lower melting point will be laminated on graphene to achieve the transfer processes [17]. As it is obvious, the shared key point in all those methods is the need to either eliminate or reduce the effect of water surface tension by providing surface support to the graphene during etching to protect the graphene in the transfer process or by decreasing the surface tension of the transfer media.

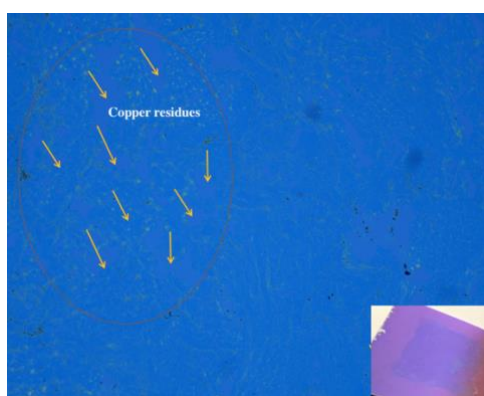


Figure 2.3 Isopropanol alcohol IPA was added to the etching solution (0.1 M of ammonium persulfate). 1:11 to reduce ST. We can see that IPA reduced the etching efficiency and led to highly copper contamination on graphene.

2.3 The effect of surface tension on graphene

The possible risk that graphene would be torn up or shrunken due to the high surface of water led to all the complications of many direct transfer techniques. Although there are not enough studies to report the effect of surface tension on graphene, most polymer-free graphene techniques were designed to avoid that possible effect. The true impact of surface tension on the direct transfer of graphene will be clarified in more detail in the following chapters.

2.4 Defective graphene

Although graphene synthesis aims to grow a large area of monolayer graphene with full coverage and less defects, the resultant graphene can be flawed by air leakage or by copper contamination under some conditions. We have done some measurements on graphene that was grown under leakage or in highly copper-contaminated tubes. As shown in Figure 2.4, the leakages, for example, would lead to creating nano-pinholes in the graphene sheet that would dramatically affect the transfer techniques. The electron mobility in this type of graphene always remains under $100 \text{ cm}^2/\text{V}\cdot\text{s}$. However, as it will be shown in the next chapter, large device intact graphene has mobility that would exceed $700 \text{ cm}^2/\text{V}\cdot\text{s}$. Surface tension can affect defective graphene, which would consequently impact the graphene transfer processes.

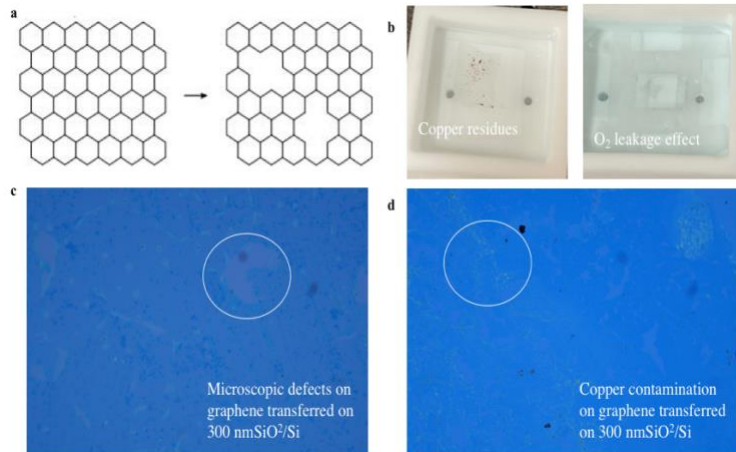


Figure 2.4 a) Defective graphene on the right vs an intact graphene structure. b) Copper residues on top of graphene after the copper substrate etched away (left) on the right, graphene edge deformation edges result of O₂ leakage. c) defective graphene transferred using polymer on SiO₂. Graphene with copper residues transferred on SiO₂. d) Graphene/ SiO₂ with copper contamination.

3 CHAPTER 3 A DIRECT SIMPLE METHOD TO TRANSFER GRAPHENE

As the chemical vapor deposition (CVD) method enables large-scale graphene synthesis, transfer technique turns out to be an essential topic [11]. Conventional polymer-assisted transfer techniques [27-29] unavoidably contaminate graphene with polymer residue and interfere with the electronic properties [30, 31]. Therefore, polymer-free direct transfer techniques are emerging to address this problem. The basic idea of the direct transfer techniques is to allow graphene to float freely on the surface of transfer liquids, and then be picked up with the target substrate directly from the liquid. Compared with the polymer-assisted methods, polymer-free transfer or direct transfer can yield a high-quality contamination-free graphene layer [17, 25, 31]. In this process, a high ST has long been believed to be destructive on monolayer graphene transfer due to the possible tearing, folding, and wrinkling [24, 25]. Thus, many efforts have focused on reducing the ST value of transfer liquid. For example, water/Isopropanol alcohol IPA mixtures are usually applied to adjust ST values [24] to ensure the success of the transfer. Nevertheless, there is, hitherto, no specific theoretical explanation or experimental demonstration to illustrate how the ST affects graphene transfer. Further, although the mechanical properties of graphene have been studied widely [32, 33] none of them clearly indicates that high ST can damage the monolayer free-floating graphene. Then, the question turns out to be whether the high ST truly damage monolayer graphene during the direct transfer, or this is just an intuitive judgment.

To answer this question, in this chapter, we explicitly explore the actual effects of the ST on graphene during the direct transfer process by tuning the ingredient of the transfer liquid and experimentally prove that graphene with good quality can always stand at high ST (ST of pure water). Further, by exchanging pure water with transfer liquids that have lower ST, we found the same graphene monolayer can sustain a broad variation in ST without showing any sign of damage.

Specifically, the same graphene layer could survive in deionized water (DI-water, with ST of 72 dyne/cm) as well as 80:20 water/IPA mixture (32 dyne/cm). This large STG of 40 dyne/cm gives us significant flexibility in selecting transfer liquid for specific applications. On the other hand, we applied STG on defective graphene and showed that the damage that occurs to the graphene at high ST results from defects in the graphene structure. Our research indicates that surface tension is not the reason causing graphene damage during the polymer-free transfer process. The feasibility of using pure water for graphene transfer significantly simplifies the transfer procedure and effectively addresses the contamination problem. Further, the large STG the high-quality graphene layers can stand provides us the extreme flexibility for selecting transfer liquids aiming at various application purposes.

3.1 Experiments:

Graphene was synthesized using the CVD method as mentioned in the first chapter. Copper foil 25 μ m thickness (CU 00035 copper foil, purity 99.99) from Goodfellow was used as a catalyst. We electropolished the copper in mainly phosphoric acid electrolyte for two minutes. Later we used DI-water and IPA sequentially to remove the acid residues (as mentioned in chapter 1). Then, the copper was launched in a quartz tube, 22 mm ID, 25mm OD. A homemade thermal CVD system was used to achieve the growth as it is mentioned in the first chapter. An image of the system can be found in the in the first chapter, Figure 1.2. The graphene growth was done at 1010 $^{\circ}$ C. The gases that were used as precursors are methane CH₄ with a flow rate of 35 sccm, and a mixture of argon and hydrogen (Ar 90%:H₂ 10%) with a flowrate 6 sccm. Later, we used O₂ plasma cleaner to etch graphene that was grown on the bottom side of the copper. Following this way, we grew monolayer graphene with full coverage [11]. However, we also grew another batch of defective graphene for the purpose of comparing the transfer results. The defective graphene can

be produced in two ways: allowing O₂ leakage during the growth or by exposing the intact graphene/copper to O₂ plasma for few seconds [34-36]. It is worth mentioning that later we replaced the regular O₂ plasma etching with radio frequency Ar plasma to improve the quality of etching and protect graphene on the upper side of ozone that might affect graphene.

3.1.1 Copper etching and Graphene Transfer.

To perform the transfer job, we designed a specific container (reactor) connected to two sided syringes to insert liquids into the reactor and pull them outside later as it is shown in Figure 3.1. This transferring cell can be used not only to achieve the transfer but also to facilitate the replacement of the liquids and enable graphene to float on liquids with different ST values. Figure. 3.2a shows a reactor which is made of Polytetrafluoroethylene (PTFE) or what is commercially known as (Teflon). During the copper etching, rinsing, and transferring processes, we used a (PET) sheet (Polyethylene Terephthalate) to make a thin film that works as a protector (retainer) as shown in Figure 3.2b. The main goal of this film is to protect graphene from any possible disturbance while exchanging the liquids. In addition, it locates the graphene piece in the same spot to ease the transfer to the target substrate later. Figure. 3.2c and d show the reactor and the retainer schematically before and after etching copper. To etch copper, we prepared a solution of (0.1 M) ammonium persulfate (CH₄)₂S₂O₈ from sigma Aldrich. The SiO₂ substrate was used in the transfer has been cleaned with a mixture of sulfuric acid and hydrogen peroxide (3:1). After rinsing with DI-water, we used O₂ plasma to enhance the substrate hydrophilicity to finalize the transfer successfully.

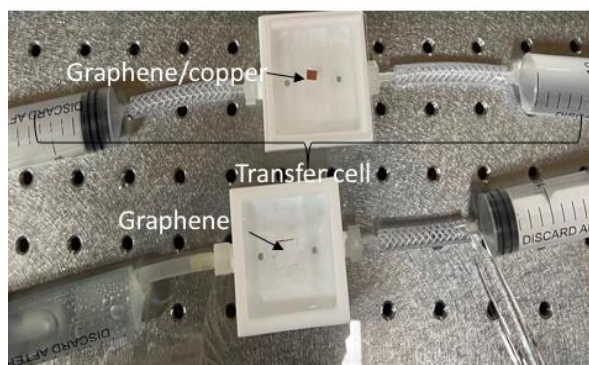


Figure 3.1. The transferring cell that designed to achieve the direct transfer of graphene including 2 sided syringes connected to the transfer reactor that made of Teflon.

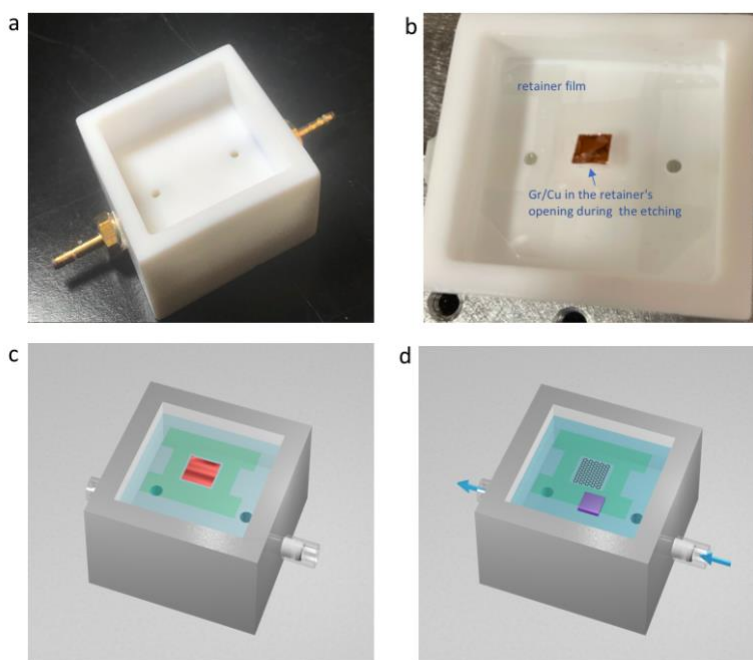


Figure 3.2 a) shows the reactor design. b) shows the reactor during the copper etching after connecting the both sided opening to the tubes. c) shows the retainer film that enclosed copper/ graphene during etching. d) schematic of graphene/copper piece enclosed by the retainer film.

3.1.2 Surface Tension Tuning

Experimentally, the ST of water can be reduced by mixing water with liquids that have lower surface tension, such as IPA or methanol. ST value of DI water is around 72 dyne/cm while ST of IPA is around 21 dyne/cm. Adding IPA to DI-water at different ratios produces mixtures with ST values lower than 72 dyne/cm and higher than 21 dyne/cm. Table.1(refer to Appendix A.1) and Figure 3.3a show the resultant ST values matching the percentages of water/IPA mixtures. To calculate the final value of the resultant ST, we measured the capillary action of each mixture (Appendix A.2). We show more detailed calculations of the capillary method in Appendix A. The ST values we calculated using the capillary experiments are compatible with the results that were measured by Rebinder and Wilhelmy (Appendix A.3). It is worth mentioning that those results are accordant too with the final ST values of the same DI-water/IPA ratios in ref[37]. The first mixture was 5% of IPA and 95 % of DI-water with a final ST 47 dyne/cm, which creates STG of 25 dyne/cm, as shown in Figure. 3.3b. We gradually increased the IPA ratio to 10 % to get final surface tension around 37 dyne/cm. Next, 20 % IPA: 80% water reduced the surface tension of water to 32 dyne/cm. Finally, we reached around 26 dyne/cm by increasing the IPA ratio to 30 %. All STG values corresponding to IPA mixtures are shown in Table.1 (in Appendix), and Figure. 3.2b. In all cases, we used capillary tubes with ID 0.25 mm to measure the capillary action of each mixture. More details can be found in the supplementary material. We filled three syringes with 30ml capacity to be used on the right side in sequence to insert the mixtures 5%,10%, then 20%, while on the left side, there is another empty syringe to drag each mix out.

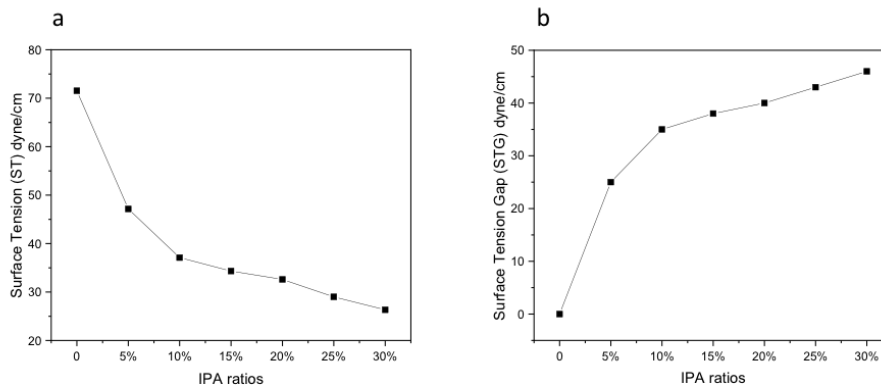


Figure 3.3 a) shows a graph of the IPA ratios and ST final values. b) Shows a graph of IPA ratios and surface tension gaps STGs.

3.1.3 Transfer Procedure

We cut an 8mm ×5 mm piece of graphene/copper that grown using CVD method, and placed one drop of IPA on the top of it. Then, gently, we placed it in the middle opening of the PET retainer. The retainer with the copper/graphene piece was placed in the reactor filled with the etching solution, as is shown in Figure. 3.2b, and 3.2c. As it is demonstrated in Figure. 3.2c and 3.2d, we can successfully replace the etching solution with pure DI-water while the graphene piece is confined in the middle opening of the PET retainer to protect it from any disturbance during the exchange of the liquids. Later, we replaced pure DI-water with a mixture of DI-water and IPA with a ratio (95%:5%). Our initial measurements indicate that the final ST of the mixture is around 47 dyne/cm, which means STG around 25 dyne/cm. Later, we increased the ratio of IPA to be 10%. In this case, the final surface tension is 37 dyne/cm, which means 35 dyne STG. Finally, we inserted a solution of DI-water/IPA with a ratio (80:20%) which reduces the ST to around 32

dyne/cm, indicating 40 STG from the initial ST of water, Table1. At this level, we inserted 300nm SiO₂/Si substrate into the reactor and aligned it underneath the graphene sheet, as illustrated in Figure 3.2d. Then, we pull out the mixture from both sides using the sided syringes that laminate graphene on the top of the substrate. Figure 3.4 a,b,c, and d show these experimental processes in sequence. Next, we repeated the above experiment, but this time we added another mixture in which we increased the IPA rate to 30%. In this case, the STG increased to 46 dyne/cm. Although this procedure raises the STG by only 6 dyne/cm extra, it produced a noticeable damage on graphene structure (images of this graphene before and after ST reduction can be found in Figure. S13a, b and c). Later, we defected graphene by enabling oxygen leakage during the graphene growth and repeated the same procedure of lowering ST gradually using DI-water/IPA mixtures with the same mentioned ratios. In this case, we noticed that graphene tore up immediately after reducing the ST from 72 dyne/cm to 47 dyne/cm (images before and after ST reduction can be found in Appendix A.4). The defective graphene shows initial defects after the copper is fully etched, such as macroscopic holes, edge deformations, and edge cracks. Those defects will be aggravated after applying STG, even at small values. This finding indicates that high ST contributed to manifesting the graphene flaws formed during the growth, while STG only exacerbated their effects. In general, graphene with less quality shows different features after the copper is fully etched, for example, edges of defective graphene deformed to a star shape, as shown in Figure. 3.4e and f. To confirm that graphene that stands high ST (ST of water) can be transferred without any sign of damage, we achieved a transfer to transmission electron microscopy (TEM) grid. For this goal, we used the lacy carbon grid on Cu with 400 mesh from Ted Pella. It is worth mentioning that in all the above experiments, the flowrate of all inserted liquids was maintained to be 1ml/2s.

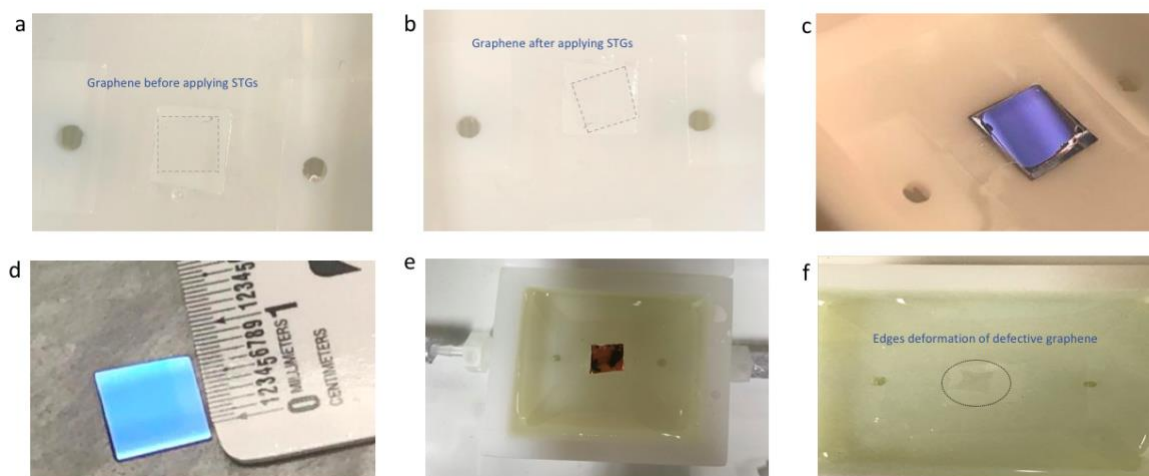


Figure 3.4 a) Graphene after replacing the etching solution with DI-water (ST 72 dyne/cm). b) graphene after applying series STGs to reach the minimum ST at 32 dyne/cm . c) A substrate had been inserted behind graphene after ST reduction to achieve the transfer. d) Graphene on 300nm SiO_2 substrate. e) Defective graphene on copper during copper etching. f) Defective graphene with edge deformations after the copper is fully etched (the original square shape changed to a star shape).

3.2 Surface Tension Effect

By performing the above procedures, we examined two different cases. Figure. 3.4a shows monolayer graphene floating on pure water before the ST reduction. Figure. 3.4b shows the same graphene sheet after reducing the ST of water by applying several STGs on it in sequence. The STG applied on graphene gradually increased from 25 dyne/cm to 40 dyne/cm. We finally transferred the graphene piece to SiO_2 substrate. During and after these processes, no sign of

damage was noticed to the graphene. In Figure. 3.4d, we can see an intact graphene piece transferred successfully on the target substrate. Obviously, this result indicates that the quality of graphene plays an important role in succeeding the direct transfer. In addition, there is no real need to achieve ST matching of the etching solution and the rinsing solution because graphene can stand STG from 25 dyne/cm to 40 dyne/cm. On the other hand, we noticed that defective graphene shows deformation after the copper is fully etched. Figure. 3.4e and f show that graphene deformed after the copper is fully etched. Obviously, we can notice that square shape of the original graphene/copper, Figure. 3.4e, changed to a star shape as a result of graphene defects as shown in Figure. 3.4f. The supplementary materials show more details of applying STG on defective graphene. We have shown that graphene with initial defects will exhibit a clear feature of deformation after reducing the ST by only adding a small amount of IPA (5%) to reduce the ST from 72 dyne/cm to 47 dyne/cm. Eventually, after increasing the amount of the lower ST liquid, we noticed that the edges were got larger cracks and small graphene pieces separated from the main graphene piece. To explain why defective graphene cannot stand STG, we suggest that an interface will be created in between the initial liquid and inserted liquid with less ST. In case graphene is defective; for example, graphene has visible cracks on the edges, the liquid interface will not only fold the graphene edges but also will find a way inside the graphene sheet because of the large cracks. Lastly, graphene will be torn into few pieces. Comparing those results with good quality graphene leads to consider that standing high ST and STG is an intrinsic feature of good quality graphene. Despite graphene can stand at high ST and STGs, it is impracticable to fully replace the DI-water (72 dyne/cm) with IPA (21dyne/cm). After making graphene floating on a liquid with ST around 32 dyne/cm, we increased the IPA ratio to 30% to reduce the ST to 26. In this case, we observed that graphene got a noticeable deformation by increasing the STG to 46

dyne/cm. In case ST reached 26 dyne/cm, graphene will be impacted no matter the quality. The detailed description of this process is as the following: When inserting a liquid mixture of 30% IPA and 70% DI-water, an interface will be created in between the initial liquid and inserted liquid with less ST. This liquid interface keeps proceeding with increasing the rate of the new liquid. This process leads to a small shrink on graphene edges. In Figure. 3.5a,b, and c, we noticed that graphene got a small shrink in the edge after inserting 25% IPA, which indicates a collapse in the graphene structure. Eventually, it tore up on the same side of the IPA mixture inserting. Since graphene tore up suddenly, we suppose that even if graphene has good quality, a few micro-cracks can still exist on the edges. They are supposed to contribute to tearing graphene while applying high STG. Those microcracks beside the interface of the two liquids can be the main reasons for tearing graphene eventually.

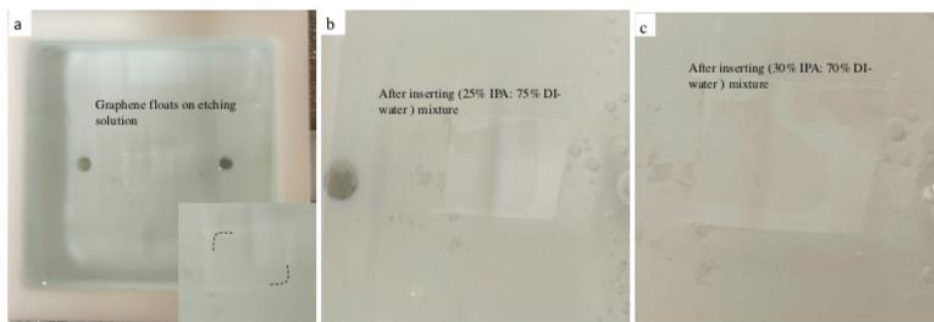


Figure 3.5 a) Shows an image of graphene before applying STG higher than 40 dyne/cm. b) Shows an image of graphene that got a small shrink after applying STG higher than 40 dyne/cm. c) Graphene tore up after applying 46 dyne/cm STG.

A similar effect can happen in case, etching solution was replaced directly with 30% IPA. The liquids interface we suggest in this discussion is also produced in all ST tuning experiments, but in STGs ≤ 40 dyne/cm, there is no damaging effect on graphene structure. However, applying

STG ≥ 46 leads to visible collapse on the graphene sheet. This result confirms that it is unachievable to replace the whole DI-water with IPA. As it is known, monolayer graphene can be determined initially by Raman signal. We measured the Raman shift of graphene that transferred after applying the maximum STG on it using a home-built confocal Raman microscopy (CRM) equipped with a tunable Argon ion laser (514.5 nm). Figure. 3.6a, indicates the Raman shift of our single-layer graphene, we can notice the exact features of single-layer graphene [38-40]; the 2D band has a sharp symmetric peak, and it is almost double the G intensity. We used atomic force microscopy (AFM) to achieve a scanning image of the graphene that transferred this way, Figure. 3.6a (inset). According to AFM scanning, the RMS roughness of graphene is around 2.9nm. Although we can notice some nano-droplets of water have been trapped in between graphene and the substrate, we avoided graphene annealing since there is no chemical residues on graphene transferred using this method [41]. Besides Raman signal and AFM, we also transferred graphene on a TEM grid. The image shown in Figure. 3.6b is a continuous single-layer graphene with no defects, transferred with pure DI-water on the 400 mesh TEM [42].

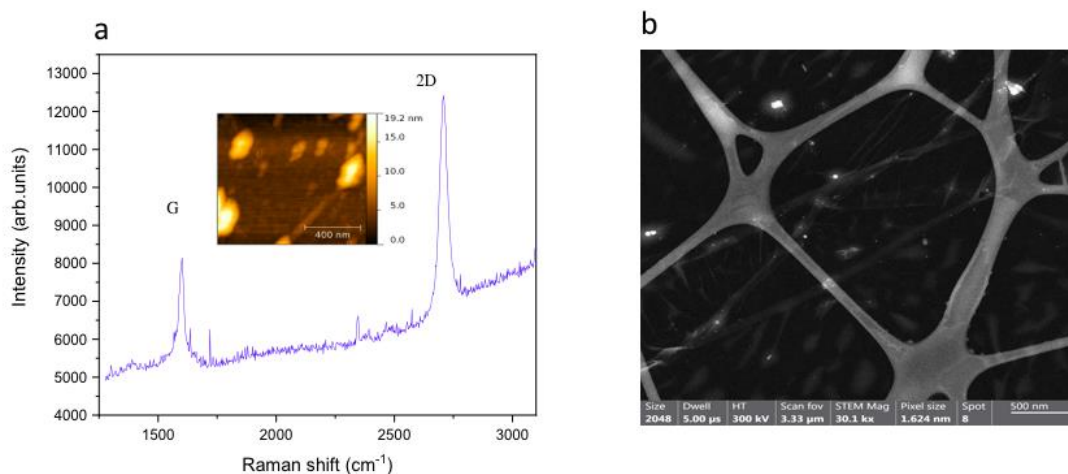


Figure 3.6 a) Raman shift of monolayer graphene transferred on 300nm SiO₂ after applying the maximum surface tension gap (40 dyne/cm). We can see that the 2D peak is almost double the G peak, which confirms that graphene is a monolayer. The inset image shows an AFM image of the same graphene with a roughness of 2.9 nm. b) TEM image of single-layer graphene transferred with pure DI-water.

3.3 Whole device transfer

After we unveiled the true impact of surface on graphene transfer, we functioned this method to achieve the whole device transfer. In more details, after chemical vapor deposition of graphene, we followed lithography manners to create patterns on graphene/Cu. A thermal evaporator was used to achieve the metal deposition (Ti: 5nm, Au: 45 nm). Next, we used acetone to accomplish the lift-off process. Later, after the copper is fully etched, we rinsed the device/graphene with only DI-water to remove the etching solution and copper residues. Finally, we removed water slowly using the sided syringes to laminate the whole device/graphene on the SiO₂ substrate, as illustrated in Figure 3.7, b, c, and d.

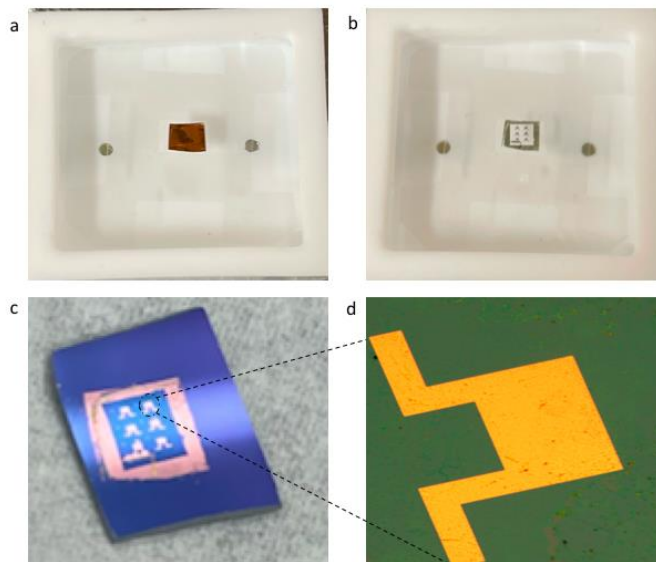


Figure 3.7 a) Device/Graphene/Cu during etching. b) Device/Graphene/Cu floating on the etching solution after copper is fully etched. c) After finalizing the transfer. d) Magnified image of the device/Graphene/SiO₂.

4 CHAPTER 4: GRAPHENE WATER MEMBARENE

Solid-state membranes, including polymethyl methacrylate PMMA [28, 29, 43], paraffin [26], and other solvable organic compound with good membrane-forming capability, have long been used for the graphene process. These membranes provide outstanding operational flexibility for the transfer process, but inevitably lead to concerns about mechanical deformation, contaminations, and trapped interfacial residues that impact the performances of graphene-based devices [44]. On the other hand, graphene process assisted with liquid membranes has rarely been explored or reported before, due to the assumption that liquid surface tension could potentially damage the graphene integrity, [24, 45] or it is impossible to establish free-standing and stable graphene-liquid membrane structures. Here, we report a newly observed graphene-water membrane (GWM) structure, which refreshes our understanding of graphene-liquid interaction, meanwhile rendering a new material process procedure. We thoroughly investigate the formation mechanism of the as-observed GWM, particularly the roles of surface tension and contact angle playing, and discover that the GWM enables a new graphene transfer method that directly renders free-suspended layer or on-substrate film with improved flatness, thanks to the high water surface tension, which has long been misinterpreted to jeopardize the graphene transfer process. Further, the GWM transfer eliminates residuals induced by conventional solid-state membranes, inspiring high-quality and contamination-free graphene process pathways toward the subsequent development of novel graphene-based electronics, [46-51] quantum devices, [52-56] micro-electromechanical systems (MEMS) [57-61], and flexible biosensors. [62, 63].

4.1 Experimental implementation of GWM

Figure 4.1a shows the optical image of the free-standing GWM structure observed in our experiment. The successful formation of the GWM requires several precautionary measures to

ensure graphene quality and integrity. The graphene employed in our study is synthesized on copper foils in a regular chemical vapor deposition (CVD) system (the growth details can be found in the first and third chapters) with a leakage rate lower than 10^{-9} bar·cm³/s to minimize defects induced by oxygen during the growth. (Figure 2.4 shows, the second chapter, defects developed when the leakage rate is higher than $>10^{-7}$ bar·cm³/s.). Following the growth, we preserve the graphene on one side of the copper foil, while etching the layer deposited on the other side with argon plasma. In this process, instead of protecting the desired surface with polymer coating, we designed a plasma treatment fixture, as demonstrated in Figure 4.1b, to shield the argon plasma for protection. The fixture consists of a top bronze clamp and a bottom copper platform with a pocket. This pocket and clamped copper foil form a Faraday cage to fully block the argon plasma from bombarding the reserved graphene layer; meanwhile, it eliminates physical contact with the delicate graphene layer and ensures its integrity. Additionally, we use argon instead of oxygen plasma for the etching because ozone generated in the oxygen plasma could potentially diffuse into the pocket and oxidize the graphene layer. These efforts ensure the graphene quality and integrity to the maximum extent for the following study on the GWM and the new transfer technique. Figure 4.1c shows graphene after etching copper and replacing the etchant with DI water.

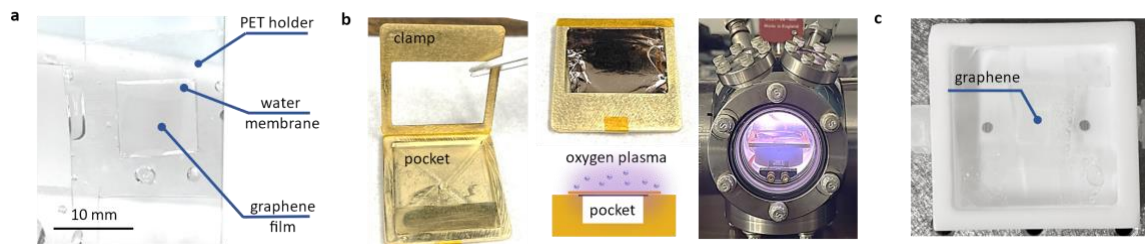


Figure 4.1 a) Free-standing GWM held by a PET frame. b) Home-designed fixture for graphene plasma removal. Copper foil with CVD graphene grown on both sides is clamped on the fixture, with one side exposed to radio-frequency plasma, while the other side is electrically shielded by the cavity formed with the copper foil and the pocket on the metal fixture. The shielded copper side has no physical contact with the surroundings, ensuring the graphene integrity. c) PTFE reactor with source and drain designed for copper etching and liquid replacement.

With the preserved graphene layer facing up, the copper foil is relocated into a specially designed reactor (Figure 4.2a), filled with a 0.1 mol/L ammonium persulfate ((NH₄)₂S₂O₈) water solution for copper etching for 3 hours, leaving monolayer graphene on the etchant surface. Due to the high surface tension of water (72 mN/m), the thin copper film and the finally released graphene float freely on the surface and are confined by a polyethylene terephthalate (PET) frame with a 1 × 1 cm² opening in the center. Subsequently, we exchanged the etchant with deionized (DI) water and rinsed the monolayer graphene several times to remove all ions, including Cu²⁺ generated during the etching step illustrated in Figure 4.2b. To avoid liquid turbulence or fluctuation during the exchange and ensure the integrity of the graphene layer, we designed inlet and outlet ports on the bottom of the reactor, through which the liquid is drained and injected at the same rate.

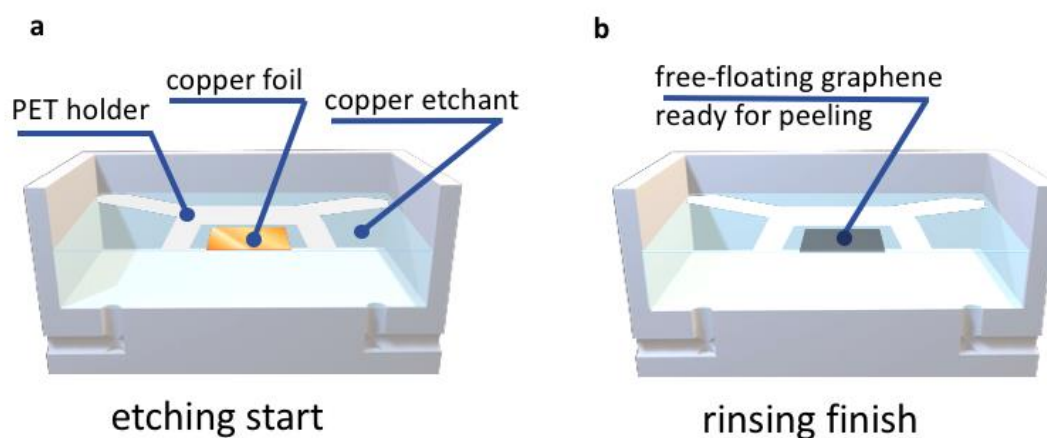


Figure 4.2 .a) The copper foil is relocated into a specially designed reactor filled with 0.1 mol/L ammonium persulfate. b) Graphene floating on pure DI-water that inserted gradually to replace etchant.

Figure 4.3. shows the free-floating graphene before and after the water exchange. A widely accepted viewpoint is that large areas of free-standing CVD graphene can be easily destroyed by pure water because of its high surface tension [24, 45]. In contrast, we did not observe any deformations generated through the entire process, suggesting CVD graphene can stand the high surface tension of DI water as long as the graphene quality is carefully preserved. Otherwise, defects developed during growth and physical damage due to improper handling indeed impair the graphene layer, bringing cracks, wrinkles, shrinking, etc., as shown in Figure 4.4.



Figure 4.3 Free-floating graphene before and after liquids exchange: On the left, graphene floating on 0.1M of ammonium persulfate. On the right, graphene floats on pure DI water.

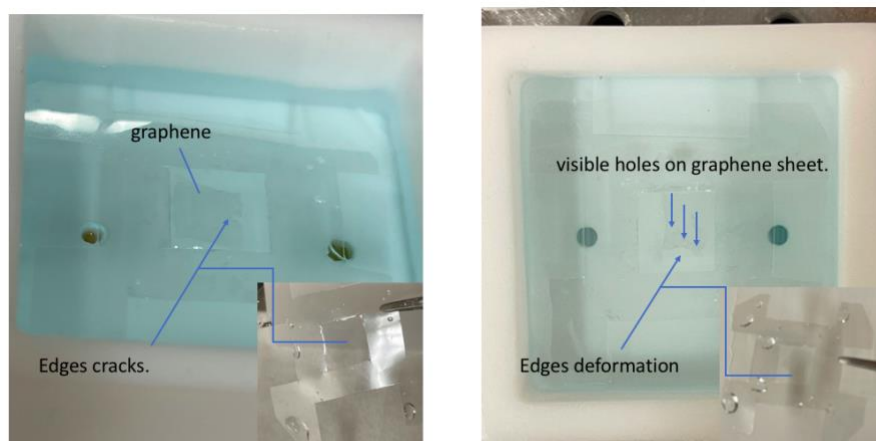


Figure 4.4 Several defects (edges deformation, shrinking, and visible holes) can be developed during the growth and jeopardize the graphene quality.

When a graphene layer is successfully isolated and freely floats on the water surface, as demonstrated in Figure 4.1c, we can readily peel the free-floating graphene layer off the water surface by lifting the PET frame from the reactor. This peeling process has been recorded in the optical image shown in Figure 4.1a. During this step, a water film bridges the graphene layer to the inner edges of the PET frame and pulls it away from the liquid surface. The film buffers the fragile graphene from the PET frame, preventing the sharp edges from piercing the atomic layer, while still distributing the necessary force for peeling. After the entire graphene layer is levered away from the water surface, the GWM showed in Figure 4.1a, 4.5a emerges.

A potential concern of the GWM is whether the large surface tension can tear the graphene layer after it is lifted from the water surface. To determine this, we performed the following analysis. The Young's modulus (E) of monolayer graphene is in the range from 1.05 to 1.1 TPa [64, 65]. Considering a graphene thickness (t) of 0.33 nm [66, 67], we can calculate the strain (ε) on monolayer graphene induced by the water surface tension (γ_{water}) via the equation [68-71]:

$$\varepsilon = \frac{2\gamma_{\text{water}}}{Et} \quad (1)$$

Equation (1) shows that the surface tension only results in a strain of 0.02%, far below the fracture strain of graphene. However, if the microscale defects, predominantly if pores or cracks are present, they can rapidly grow under strain and cause brittle fractures to the polycrystal CVD graphene. Thus, the formation and stability of the GWM strongly depend on the quality of the graphene layer rather than the water surface tension.

4.2 Theoretical modeling of GWM

To understand the peeling process, we established a mechanical peeling model considering two

dominating factors that determine a successful peeling: the driving force provided by the water film that bridges the graphene and the inner edges of the PET frame and helps peel off graphene, and the adhesion between the graphene layer and liquid surface to be overcome during peeling. The driving force per unit width (D) is provided by the surface tension (γ_l) of water in the form of $D = 2\gamma_l$. The force per unit width (P) required to peel the graphene can be derived from the energy balance between the work done by the peeling force and the variation of graphene/liquid interfacial energy [72, 73],

$$P = \frac{\gamma_l \times (1 + \cos\theta_{sl})}{1 - \cos\alpha} \quad (2),$$

where θ_{sl} denotes the contact angle between graphene and water, and α labels the peeling angle as defined in Figure 4.5(b) inset. For a successful peel, we will have $D \geq P$, i.e.,

$$\alpha \geq \arccos\left[\frac{1 - \cos\theta_{sl}}{2}\right] \quad (3),$$

For DI water on graphene, we experimentally determined the contact angle of 100° (Figure 4.5c) by using a goniometer (DataPhysics OCA 15EC), which takes place within the reported range of $95\sim 100^\circ$ [74, 75]. Theoretical prediction resulting from Equation (3) shows a minimum peeling angle of 54.1° for a successful peeling of graphene from the water surface. This is consistent with the experimental observation of 54.6° shown in Figure 4.5a. Figure 4.5b summarizes the diagram for picking up the graphene from a liquid surface. A smaller contact angle associated with stronger hydrophilicity between graphene and liquid will require a more powerful driving force and thus a larger peeling angle for a successful graphene lifting.

Additionally, we perform molecular dynamics (MD) simulations on the entire peeling process. A graphene film with $4 \text{ nm} \times 10 \text{ nm}$ was placed on the surface of the liquid and peeled by applying a mechanical force with the peeling angle of 57.5° at a velocity of 1 nm/ns . Figure 4.5d shows the

simulation snapshots of peeling graphene from water at 0, 3.5, and 6.0 ns, suggesting a neat peeling of graphene film without liquid molecular residues on the peeled graphene. Figure 4.5e further plots the evolution of the peeling force as a function of peeling time and implies an equilibrium has been achieved 4 ns after the peeling began. The peeling force at the steady-state is 115.5 mN/m when pure water is employed, agreeing with the theoretical prediction of 128.6 mN/m by Equation (3) with water surface tension of 72 mN/m [76, 77].

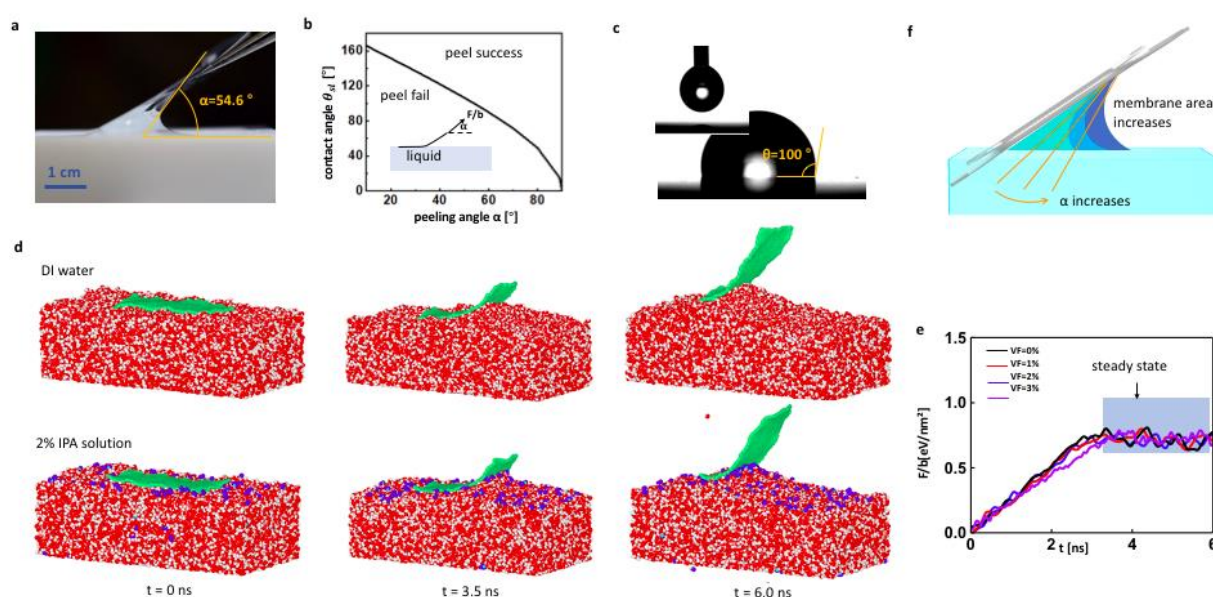


Figure 4.5 a) Optical image of the graphene peeling process with a peeling angle of 54.6° when pure DI water is employed. b) Criteria of success peeling. The required minimum peeling angle increases and the liquid contact angle decreases (i.e., the liquid become more hydrophilic). When the configuration falls in the successful range, the graphene-water membrane can readily form and be isolated from the liquid surface. If in the failure zone, the membrane breaks. Inset: the definition of peeling angle. c) Contact angle measurement of water on a graphene surface. d) Molecular dynamics simulation of the graphene peeling process. The figures illustrate the frames of the dynamics at 0, 3.5, and 6 s after the peeling starts. The peeling angle is set at 57.5° to ensure a successful peeling in the simulation. e) Simulated evolution of the peeling force as a function of time and IPA concentration. f) A smaller contact angle (induced by higher IPA concentration) requires a larger peeling angle and thus, increases the surface area of the liquid membrane,

increasing the risk of membrane breaking and peeling failure.

Besides the DI water, we also consider the peeling process when IPA is added to the water to comprehend the effects of lower surface tension and contact angle. Experimentally, we successfully peeled the graphene layers out of 1% and 2% IPA solution with peeling angles of 55.5° and 57.0° , respectively, which further confirms the theoretical prediction of the “successful peel” region shown in Figure 4.5c, (as shown in Figure 4.6). MD simulations also indicate that the peeled graphene remains clean without residual IPA molecules, similar to peeling from the water surface, as shown in Figure 4.5d. As the IPA concentrate increases to 3%, the liquid (water with 3% IPA) membrane breaks before the graphene is fully peeled off. Consequently, the entire process fails because a higher IPA concentration decreases the contact angle and necessitates a larger peeling angle, which in turn stretches the liquid membrane until it breaks before the whole graphene layer is lifted from the liquid surface, as illustrated in Figure 4.5f. Quantitatively, our MD simulation finds that a 3% IPA solution leads to a 94.5° contact angle and requires at least a 57.4° peeling angle, which will break the liquid membrane between frame and graphene and fail to pick up the graphene. The peeling force remains approximately the same as a small amount of IPA barely influences the contact angle of the water, as suggested by the theoretical predictions shown in appendix B.

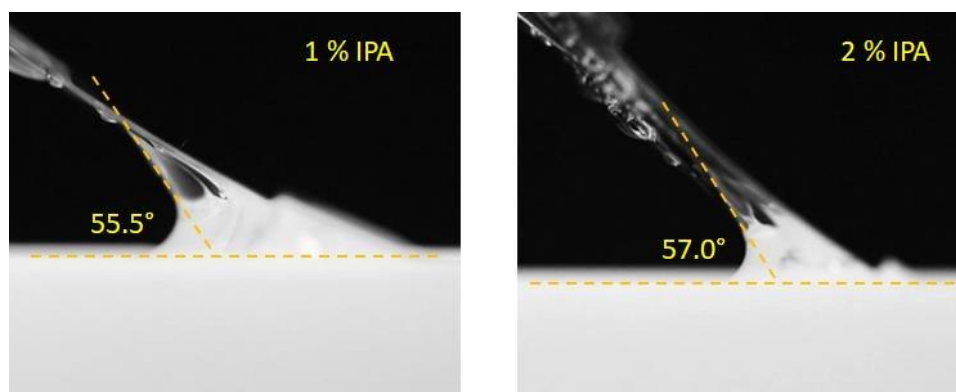


Figure 4.6 A successful peeling of GWM from a liquid contains 1% IPA to 99% DI water (left), and a liquid contains 2% IPA to 98% DI water (right).

The discussed experimental and theoretical analyses indicate that high-quality graphene can readily stand the high surface tension of water. Interestingly, leveraging the large contact angle between graphene and water (i.e., high hydrophobicity), a stable GWM forms when free-floating graphene is peeled out of the water surface with a frame structure. This observation refreshes our understanding of graphene-water interaction and exhibits a new hybrid membrane structure that inspires us with a new large-scale polymer-free graphene process technique with excellent outcomes.

4.3 GWM-enabled one-step graphene suspension with no polymer residues

One obvious benefit of this GWM is the ensured cleanness of the graphene layer by eliminating the usage of PMMA or other supporting media for processing. Thus, small organic molecules dispersed in the air turn out to be the only contamination source, which can be readily removed by afterward annealing. Indeed, the transition electron microscopy (TEM) image shown in Figure 4.7b reveals a very clean graphene surface rendered by the GWM, and the scanning TEM (STEM) can clearly distinguish individual carbon atoms.

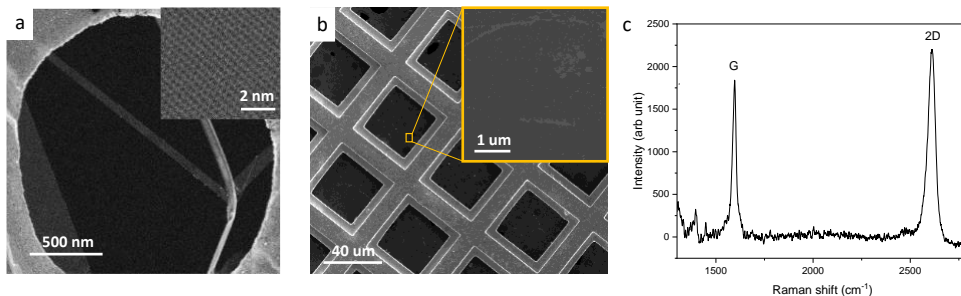


Figure 4.7 a) STEM image of graphene transferred with GWM. The low-resolution image shows clean graphene surface, and the high-resolution image (inset) clearly distinguish carbon atoms. b) SEM image of free-suspended graphene directly produced by the GWM, and the magnified image (inset) shows no contamination. c) Raman spectrum of the free-suspended graphene.

Besides the ultra-cleanness, another striking significance of the GMW distinct from other process methods is a one-step and direct graphene suspension without any assistance of supporting media or supercritical drying employed in earlier studies. [78],[79] Figure 4.7c shows the scanning electron microscopy image of a graphene suspension directly obtained by transferring a GMW on a mesh TEM grid with $40 \times 40 \mu\text{m}^2$ openings. The inset magnification exhibits the uniform and flawless graphene layer. This one-step graphene suspension can be attributed to the high graphene quality, and more importantly, the reduced amount of water adhered to the graphene surface when the GMW forms, as indicated by our molecular dynamics simulation that no water adheres to the graphene layer (Figure 4.5d and Figure 4.8) when the GWM is peeled from the water surface. Therefore, the GWM can drastically simplify the procedure for large-scale suspended graphene and other 2D material structure constructions.

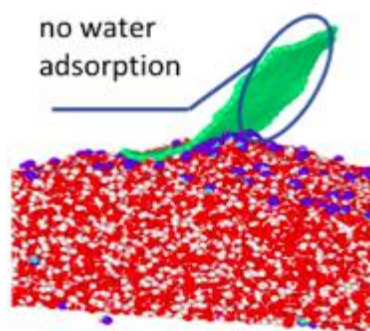


Figure 4.8 MD simulation confirms that water molecules do not adhere to the graphene layer being peeled off.

Based on the free-suspended graphene, we also performed Raman characterization, as shown in Figure 4.7c, which shows no signal of amorphous carbon. [80] The reduced 2D/G peak ratio is well-known for free-standing graphene that is charge neutral, [81], [82] further suggesting the contamination-free surface of the graphene produced by the GWM.

4.4 GWM-enabled high-quality graphene transfer on substrates

The GWM can also be leveraged for graphene transfer onto many types of substrates. Briefly, we can readily pick up the free-floating graphene layer from the water surface with the PET retainer, then align and laminate it onto the target substrate, as shown in Figure 4.9a. Here, we employ Si wafers with a 300 nm SiO₂ layer as the substrates to perform the transfer experiment. They are cleaned with piranha solution (H₂SO₄: H₂O₂ (37%) =4:1) to remove organic residues thoroughly. Figure 4.9b inset shows the optical image of high-quality large-area graphene transfer performed with the above procedure, indicating that the sample's integrity is fully preserved without visually detectable cracking or wrinkling. The Raman spectroscopy measurement (Figure 4.9b) clearly distinguishes the sharp G and 2D peaks with an intensity ratio of 1:2, whereas the D peak is very

weak. These observations indicate the monolayer graphene with excellent quality [64, 83]. To further confirm the microscopic structure and flatness, we conducted atomic force microscopy AFM study on the graphene transferred with our new method and confirmed a low morphology roughness (i.e., the root mean square RMS of the surface height) of 1.5 nm, as demonstrated in Figure 4.9c. Graphene grain boundaries can also be clearly distinguished on the AFM image. In comparison, the transfer following the previously reported polymer-free method (Figure 4.9d) results in the roughness of 3.4 nm, as shown in Figure 4.9e.

One primary reason for this drastic improvement can be attributed to the water film, which bridges the PET frame and graphene layer while stretching and flattening the atomic layer with its surface tension, as explained by Equation (1). Another reason for the much higher transfer quality results from less liquid being trapped on the graphene-substrate interface in our procedure than in the conventional polymer-free transfer technique, as confirmed by MD simulations in Figure 4.5d. In the previously reported polymer-free transfer methods [24-26], target substrates are typically fully merged into the transfer liquid (water or IPA mixture, as illustrated in Figure 4.9d).

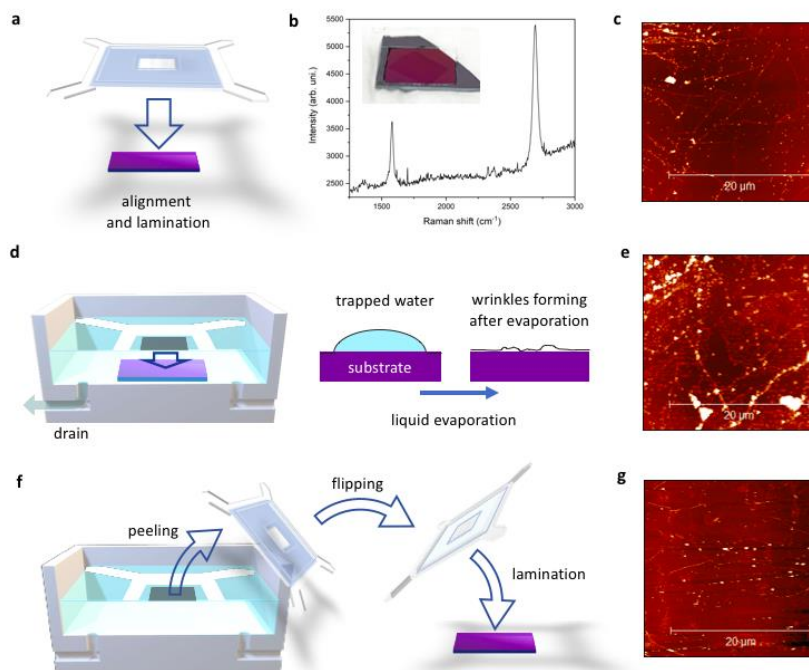


Figure 4.9 a) Graphene-wafer membrane for transfer. b) Raman spectrum of the as-transferred graphene. Inset: Optical image of the as-transferred graphene. c) AFM image of graphene transferred on Si/SiO₂ wafer with graphene-water membrane. d) Conventional graphene transfer method with target-substrate merged into liquid. The liquid is drawn out of the reactor to lower graphene and laminate it onto the substrate. Because there is liquid trapped on the graphene-substrate interface, wrinkle develops after the liquid evaporates. e) AFM image of graphene transferred onto Si/SiO₂ wafer with the conventional polymer-free procedure. f) Graphene transfer procedure with flipped graphene-water membrane to further eliminate water trapping on interfaces. g) AFM image of the flipping transfer with better flatness and transfer quality.

Then, the liquid is drained out of the container to lower the graphene layer until it is in contact with the target. This procedure inevitably creates multiple pockets of trapped liquid on the graphene-substrate interface. Even after the trapped water eventually evaporates, folding,

wrinkling, or other deformations persist, as illustrated in Figure 4.9d, and lead to the as-observed RMS roughness of 3.4 nm. This problem is detrimental to the afterward device fabrication and test. Nevertheless, our approach can be effectively addressed in such a manner that the hydrophobic nature of graphene repels most of the water accumulated underneath the layer unless minor residuals are anchored by hydrophilic functional groups, including hydroxyl [75], due to unintentional graphene oxidation. Undeniably, our MD simulation further confirms that water molecules do not adhere to the graphene layer being peeled off, as shown in Figure 4.8, even if IPA is added and lowers the graphene contact angle. To eliminate the minor interfacial residues or contaminations, we can flip the entire PET frame with a graphene-water membrane and laminate the “dry” surface onto the substrates. Figure 4.9f showcases the workflow of this flip-transfer method. By doing so, we find that the roughness of the resulting transfer is improved to 0.7 nm (Figure 4.9g), which is close to the intrinsic roughness of SiO₂ (0.4 nm) used in our study. The improvement in graphene flatness drastically enhances its electronic performance. For example, compared with the conventional polymer-free transfer method shown in Figure 4.9d, our GWM-transfer doubles the FET mobility, as illustrated in Figure 4.10, suggesting it can serve as a promised method for high-quality electronic device fabrication. It is worth mentioning that shadow masks were employed for graphene channel etching and electrode deposition to avoid the usage of photoresist, which could bring residues and uncertainties that interfere with the comparison. As a tradeoff, our FET channels have a relatively large size of 1 mm × 4 mm, which makes the scattering on graphene grain boundary and substrate interfaces more significant, as such lowering the absolute mobility value. On the other hand, this large-scale design averages the local mobility fluctuation induced by the above factors, and makes our conclusion of mobility enhancement more statistically convincing, compared with micrometer-scale devices. Additionally, the Dirac cone

feature can be clearly distinguished even in these large-scale FET devices, confirming the high quality of our transfer methods.

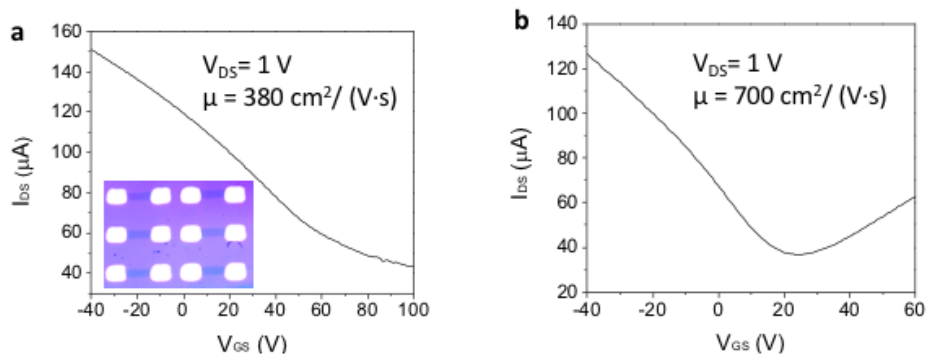


Figure 4.10 Field-effect transistors ((a) inset) had been fabricated with the same batch of graphene layers transferred with the conventional and our newly developed polymer-free transfer approach. The FET made with the conventional polymer-free method (a) yields mobility of $380 \text{ cm}^2\text{V}^{-1}\text{s}^{-1}$, whereas our new method renders a significant improvement up to $700 \text{ cm}^2\text{V}^{-1}\text{s}^{-1}$ as shown in (b).

Aside from the interpretation of the surface tension effect on the peeling processes, we also identified the substrate factors, particularly the hydrophilicity effect on the success and quality of our new transfer method. Accordingly, we notice that a hydrophilic substrate can sufficiently sustain the integrity of the water membrane and thus the graphene layer. The water keeps tensioning the graphene layer until it fully volatilizes and leaves a highly flat morphology. However, if the substrate is highly hydrophobic, the water film bridging collapses and drags the entire graphene layer to one side of the PET frame instantaneously when it touches the surface, failing the transfer, as illustrated in Figure 4.11a. To overcome this problem and enable the transfer onto a hydrophobic substrate, a hydrophilic frame surrounding the hydrophobic area is introduced to stabilize the graphene-water film and sustain the tension until the transfer is finished, as

demonstrated in Figure 4.11b. For example, a SiO₂ frame was patterned on Si substrate (Figure 4.11c) through a thermal oxidation process for transferred and form Si-graphene junction.

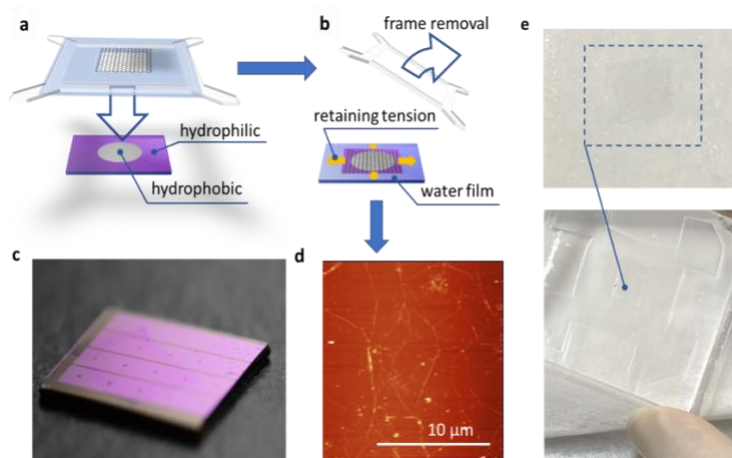


Figure 4.11 (a) Graphene-water membrane transfer onto a hydrophobic substrate with the assistant of a hydrophilic frame. (b) The hydrophilic frame holds the water and retains the tension that flattens the graphene layer until the graphene layer is laminated firmly onto the substrate. (c) Optical image of graphene transferred onto silicon with SiO₂ frame severing as a hydrophilic frame. (d) AFM image of as-transferred graphene on the silicon surface shown in (c). (e) Graphene layer transferred on the hydrogel. (1 g of agar and 0.2 g gelatin dissolved in 100 ml DI water).

The entire substrate was treated with hydrogen fluoride acid (5% aqueous solution) before the transfer to passivate the silicon area with hydrogen atoms and produce a hydrophobic surface, whereas the SiO₂ frame remains hydrophilic. With the assistance of this frame, we successfully transferred graphene onto the Si and obtained ultra-high flatness, as verified by the AFM image in Figure 4.11d. Other hybrid structures can also be produced with the same method. Further, Figure

4.11e illustrates that our newly developed method can effectively transfer graphene to other unconventional substrates, such as hydrogel and other soft-matters, whereas earlier polymer-assisted or polymer-free methods are infeasible because the organic solvent for the afterward cleaning or the full liquid transfer environment can easily damage the hydrogel structure. Therefore, our method also facilitates the fabrication of large-scale hybrid structures of graphene and soft matters for the applications of biosensors, wearable devices, and many more [46].

CONCLUSION

Graphene with good quality can stand high ST, while defective graphene does not show the same feature. Matching surface tension values of the etching solution and rinsing liquid has no importance because, experimentally, graphene could stand a maximum surface tension gap around 40 dyne/cm. Based on these results, no need to reduce the water surface tension to achieve the direct transfer of graphene, as long as high sample quality is ensured. Our observation removes the long-standing illusion that high ST can damage graphene during the polymer-free transfer process. Beside this method, we report a new GWM structure and analyze its forming mechanisms and prerequisites from the perspectives of experimental observation, theoretical models, and MD simulations. It is found that the water plays an essential role by providing critical buffering between fragile graphene layers and sharp PET frame for graphene peeling. Also, the large surface tension and contact angle of water deliver sufficient peeling force to isolate graphene layer from the water surface, facilitating the forming of a GWM. Based on this newly observed GWM, we also developed an alternative large graphene transfer method with drastically improved transfer flatness and electronic performances, in part due to the high surface tension of water, which retains the graphene flatness through the entire pickup, alignment, and lamination workflow. These benefits provide an alternative approach for high-performance device fabrication based on graphene and other low-dimensional materials.

REFERENCES

1. Novoselov, K.S., et al., *Electric field effect in atomically thin carbon films*. science, 2004. **306**(5696): p. 666-669.
2. Bhuyan, M., et al., *Synthesis of graphene*. International Nano Letters, 2016. **6**(2): p. 65-83.
3. Kim, D.J., et al., *Degradation protection of color dyes encapsulated by graphene barrier films*. Chemistry of Materials, 2019. **31**(18): p. 7173-7177.
4. Huang, X., et al., *Graphene-based electrodes*. Advanced Materials, 2012. **24**(45): p. 5979-6004.
5. Novoselov, K.S., et al., *Room-temperature quantum Hall effect in graphene*. science, 2007. **315**(5817): p. 1379-1379.
6. Geim, A.K., *Graphene: status and prospects*. science, 2009. **324**(5934): p. 1530-1534.
7. Bartzill, M., *The surface science of graphene: Metal interfaces, CVD synthesis, nanoribbons, chemical modifications, and defects*. Surface Science Reports, 2012. **67**(3-4): p. 83-115.
8. Wintterlin, J. and M.-L. Bocquet, *Graphene on metal surfaces*. Surface Science, 2009. **603**(10-12): p. 1841-1852.
9. Hong, G., et al., *On the mechanism of hydrophilicity of graphene*. Nano letters, 2016. **16**(7): p. 4447-4453.
10. Zhu, Y., et al., *Graphene and graphene oxide: synthesis, properties, and applications*. Advanced materials, 2010. **22**(35): p. 3906-3924.
11. Li, X., et al., *Large-area synthesis of high-quality and uniform graphene films on copper foils*. science, 2009. **324**(5932): p. 1312-1314.
12. Gao, M., et al., *Epitaxial growth and structural property of graphene on Pt (111)*. Applied Physics Letters, 2011. **98**(3): p. 033101.
13. Yang, W., et al., *Epitaxial growth of single-domain graphene on hexagonal boron nitride*. Nature materials, 2013. **12**(9): p. 792-797.
14. Camara, N., et al., *Selective epitaxial growth of graphene on SiC*. Applied Physics Letters, 2008. **93**(12): p. 123503.
15. Hwang, J., et al., *van der Waals epitaxial growth of graphene on sapphire by chemical vapor deposition without a metal catalyst*. Acs Nano, 2013. **7**(1): p. 385-395.
16. Reina, A., et al., *Transferring and identification of single-and few-layer graphene on arbitrary substrates*. The Journal of Physical Chemistry C, 2008. **112**(46): p. 17741-17744.
17. Martins, L.G., et al., *Direct transfer of graphene onto flexible substrates*. Proceedings of the National Academy of Sciences, 2013. **110**(44): p. 17762-17767.
18. Okmi, A., et al., *How surface tension matters in polymer-free graphene transfer*. Oxford Open Materials Science, 2021. **1**(1): p. itab007.
19. Okmi, A., et al., *Discovery of Graphene-Water Membrane Structure: Toward High-Quality Graphene Process*. Advanced Science, 2022: p. 2201336.
20. Li, D., et al., *An in-situ study of copper electropolishing in phosphoric acid solution*. Int. J. Electrochem. Sci, 2013. **8**(1): p. 1041.
21. Zhan, L., et al., *Preparation of ultra-smooth cu surface for high-quality graphene synthesis*. Nanoscale Research Letters, 2018. **13**(1): p. 1-6.

22. Vlassiouk, I., et al., *Large scale atmospheric pressure chemical vapor deposition of graphene*. Carbon, 2013. **54**: p. 58-67.
23. Regan, W., et al., *A direct transfer of layer-area graphene*. Applied Physics Letters, 2010. **96**(11): p. 113102.
24. Lin, W.-H., et al., *A direct and polymer-free method for transferring graphene grown by chemical vapor deposition to any substrate*. ACS nano, 2014. **8**(2): p. 1784-1791.
25. Zhang, G., et al., *Versatile polymer-free graphene transfer method and applications*. ACS applied materials & interfaces, 2016. **8**(12): p. 8008-8016.
26. Leong, W.S., et al., *Paraffin-enabled graphene transfer*. Nature communications, 2019. **10**(1): p. 1-8.
27. Barin, G.B., et al., *Optimized graphene transfer: Influence of polymethylmethacrylate (PMMA) layer concentration and baking time on graphene final performance*. Carbon, 2015. **84**: p. 82-90.
28. Jia, Y., et al., *Toward high carrier mobility and low contact resistance: laser cleaning of PMMA residues on graphene surfaces*. Nano-micro letters, 2016. **8**(4): p. 336-346.
29. Gong, C., et al., *Rapid selective etching of PMMA residues from transferred graphene by carbon dioxide*. The Journal of Physical Chemistry C, 2013. **117**(44): p. 23000-23008.
30. Suk, J.W., et al., *Enhancement of the electrical properties of graphene grown by chemical vapor deposition via controlling the effects of polymer residue*. Nano letters, 2013. **13**(4): p. 1462-1467.
31. Ahn, Y., et al., *Procedure of removing polymer residues and its influences on electronic and structural characteristics of graphene*. Applied Physics Letters, 2013. **102**(9): p. 091602.
32. Zhao, H., K. Min, and N.R. Aluru, *Size and chirality dependent elastic properties of graphene nanoribbons under uniaxial tension*. Nano letters, 2009. **9**(8): p. 3012-3015.
33. Liu, Y., et al., *Mechanical properties of graphene papers*. Journal of the Mechanics and Physics of Solids, 2012. **60**(4): p. 591-605.
34. Cui, Y., et al., *Dynamic characterization of graphene growth and etching by oxygen on Ru (0001) by photoemission electron microscopy*. The Journal of Physical Chemistry C, 2009. **113**(47): p. 20365-20370.
35. Sanyal, B., et al., *Molecular adsorption in graphene with divacancy defects*. Physical Review B, 2009. **79**(11): p. 113409.
36. Gurel, H.H., V.O. Ozçelik, and S. Ciraci, *Dissociative adsorption of molecules on graphene and silicene*. The Journal of Physical Chemistry C, 2014. **118**(47): p. 27574-27582.
37. Park, J.-G., et al., *Interfacial and electrokinetic characterization of IPA solutions related to semiconductor wafer drying and cleaning*. Journal of the Electrochemical society, 2006. **153**(9): p. G811.
38. Ni, Z., et al., *Raman spectroscopy and imaging of graphene*. Nano Research, 2008. **1**(4): p. 273-291.
39. John, R., et al., *Sequential electrochemical unzipping of single-walled carbon Nanotubes to graphene ribbons revealed by in situ raman spectroscopy and imaging*. ACS nano, 2014. **8**(1): p. 234-242.
40. Graf, D., et al., *Raman imaging of graphene*. Solid State Communications, 2007. **143**(1-2): p. 44-46.

41. Cheng, Z., et al., *Toward intrinsic graphene surfaces: a systematic study on thermal annealing and wet-chemical treatment of SiO₂-supported graphene devices*. Nano letters, 2011. **11**(2): p. 767-771.
42. Wilson, N.R., et al., *Weak mismatch epitaxy and structural feedback in graphene growth on copper foil*. Nano Research, 2013. **6**(2): p. 99-112.
43. Kaplas, T., et al., *Transfer and patterning of chemical vapor deposited graphene by a multifunctional polymer film*. Applied Physics Letters, 2018. **112**(7): p. 073107.
44. Chen, Y., X.L. Gong, and J.G. Gai, *Progress and challenges in transfer of large-area graphene films*. Advanced science, 2016. **3**(8): p. 1500343.
45. Zhang, X., et al., *A scalable polymer-free method for transferring graphene onto arbitrary surfaces*. Carbon, 2020. **161**: p. 479-485.
46. Kang, J., et al., *Graphene transfer: key for applications*. Nanoscale, 2012. **4**(18): p. 5527-5537.
47. Yang, X. and M. Yan, *Removing contaminants from transferred CVD graphene*. Nano Research, 2020. **13**(3): p. 599-610.
48. Avouris, P. and F. Xia, *Graphene applications in electronics and photonics*. Mrs Bulletin, 2012. **37**(12): p. 1225-1234.
49. Avouris, P. and C. Dimitrakopoulos, *Graphene: synthesis and applications*. Materials today, 2012. **15**(3): p. 86-97.
50. Jang, H., et al., *Graphene-based flexible and stretchable electronics*. Advanced Materials, 2016. **28**(22): p. 4184-4202.
51. Kostarelos, K. and K.S. Novoselov, *Graphene devices for life*. Nature nanotechnology, 2014. **9**(10): p. 744-745.
52. Lin, L., et al., *Towards super-clean graphene*. Nature communications, 2019. **10**(1): p. 1-7.
53. Engels, S., et al., *Fabrication of coupled graphene–nanotube quantum devices*. Nanotechnology, 2012. **24**(3): p. 035204.
54. Weitz, R.T. and A. Yacoby, *Graphene rests easy*. Nature nanotechnology, 2010. **5**(10): p. 699-700.
55. Westervelt, R., *Graphene nanoelectronics*. Science, 2008.
56. Dragoman, M. and D. Dragoman, *Graphene-based quantum electronics*. Progress in Quantum Electronics, 2009. **33**(6): p. 165-214.
57. Fan, X., et al., *Manufacture and characterization of graphene membranes with suspended silicon proof masses for MEMS and NEMS applications*. Microsystems & Nanoengineering, 2020. **6**(1): p. 1-17.
58. Martin-Olmos, C., et al., *Graphene MEMS: AFM probe performance improvement*. ACS nano, 2013. **7**(5): p. 4164-4170.
59. Zang, X., et al., *Graphene and carbon nanotube (CNT) in MEMS/NEMS applications*. Microelectronic Engineering, 2015. **132**: p. 192-206.
60. Ahmadian, M., K. Jafari, and M.J. Sharifi, *Novel graphene-based optical MEMS accelerometer dependent on intensity modulation*. ETRI Journal, 2018. **40**(6): p. 794-801.
61. Engel, M., et al., *Light–matter interaction in a microcavity-controlled graphene transistor*. Nature communications, 2012. **3**(1): p. 1-6.
62. Morales-Narváez, E., et al., *Graphene-based biosensors: going simple*. Advanced Materials, 2017. **29**(7): p. 1604905.

63. Yang, Y., et al., *Ultrafine graphene nanomesh with large on/off ratio for high-performance flexible biosensors*. *Advanced Functional Materials*, 2017. **27**(19): p. 1604096.
64. Lee, J.-U., D. Yoon, and H. Cheong, *Estimation of Young's modulus of graphene by Raman spectroscopy*. *Nano letters*, 2012. **12**(9): p. 4444-4448.
65. Lee, C., et al., *Measurement of the elastic properties and intrinsic strength of monolayer graphene*. *science*, 2008. **321**(5887): p. 385-388.
66. Ni, Z., et al., *Graphene thickness determination using reflection and contrast spectroscopy*. *Nano letters*, 2007. **7**(9): p. 2758-2763.
67. Green, A.A. and M.C. Hersam, *Solution phase production of graphene with controlled thickness via density differentiation*. *Nano letters*, 2009. **9**(12): p. 4031-4036.
68. Zhang, P., et al., *Fracture toughness of graphene*. *Nature communications*, 2014. **5**(1): p. 1-7.
69. Shekhawat, A. and R.O. Ritchie, *Toughness and strength of nanocrystalline graphene*. *Nature communications*, 2016. **7**(1): p. 1-8.
70. Jung, G., Z. Qin, and M.J. Buehler, *Molecular mechanics of polycrystalline graphene with enhanced fracture toughness*. *Extreme Mechanics Letters*, 2015. **2**: p. 52-59.
71. Zhang, Y., et al., *Capillary transfer of soft films*. *Proceedings of the National Academy of Sciences*, 2020. **117**(10): p. 5210-5216.
72. Zhang, Y., Q. Liu, and B. Xu, *Liquid-assisted, etching-free, mechanical peeling of 2D materials*. *Extreme Mechanics Letters*, 2017. **16**: p. 33-40.
73. Zhang, Y., et al., *Chemomechanics of transfer printing of thin films in a liquid environment*. *International Journal of Solids and Structures*, 2019. **180**: p. 30-44.
74. Taherian, F., et al., *What is the contact angle of water on graphene?* *Langmuir*, 2013. **29**(5): p. 1457-1465.
75. Feng, J. and Z. Guo, *Wettability of graphene: from influencing factors and reversible conversions to potential applications*. *Nanoscale horizons*, 2019. **4**(2): p. 339-364.
76. Hauner, I.M., et al., *The dynamic surface tension of water*. *The journal of physical chemistry letters*, 2017. **8**(7): p. 1599-1603.
77. Floriano, M. and C. Angell, *Surface tension and molar surface free energy and entropy of water to -27.2. degree*. *C. Journal of Physical Chemistry*, 1990. **94**(10): p. 4199-4202.
78. Yulaev, A., et al., *Toward clean suspended CVD graphene*. *RSC advances*, 2016. **6**(87): p. 83954-83962.
79. Fu, J., et al., *Advanced transferring of large-area freestanding graphene films by using fullerenes*. *Nanotechnology*, 2019. **30**(26): p. 26LT01.
80. Lin, Y.-C., et al., *Graphene annealing: how clean can it be?* *Nano letters*, 2012. **12**(1): p. 414-419.
81. Casiraghi, C., *Doping dependence of the Raman peaks intensity of graphene close to the Dirac point*. *Physical Review B*, 2009. **80**(23): p. 233407.
82. Mohiuddin, T., et al., *Uniaxial strain in graphene by Raman spectroscopy: G peak splitting, Grüneisen parameters, and sample orientation*. *Physical Review B*, 2009. **79**(20): p. 205433.
83. Banszerus, L., et al., *Identifying suitable substrates for high-quality graphene-based heterostructures*. *2D Materials*, 2017. **4**(2): p. 025030.
84. Plimpton, S., P. Crozier, and A. Thompson, *LAMMPS-large-scale atomic/molecular massively parallel simulator*. *Sandia National Laboratories*, 2007. **18**: p. 43.

85. Stuart, S.J., A.B. Tutein, and J.A. Harrison, *A reactive potential for hydrocarbons with intermolecular interactions*. The Journal of chemical physics, 2000. **112**(14): p. 6472-6486.
86. Brenner, D.W., et al., *A second-generation reactive empirical bond order (REBO) potential energy expression for hydrocarbons*. Journal of Physics: Condensed Matter, 2002. **14**(4): p. 783.
87. Berendsen, H.J., et al., *Molecular dynamics with coupling to an external bath*. The Journal of chemical physics, 1984. **81**(8): p. 3684-3690.
88. Chen, B., J.J. Potoff, and J.I. Siepmann, *Monte Carlo calculations for alcohols and their mixtures with alkanes. Transferable potentials for phase equilibria. 5. United-atom description of primary, secondary, and tertiary alcohols*. The Journal of Physical Chemistry B, 2001. **105**(15): p. 3093-3104.
89. Werder, T., et al., *On the water– carbon interaction for use in molecular dynamics simulations of graphite and carbon nanotubes*. The Journal of Physical Chemistry B, 2003. **107**(6): p. 1345-1352.
90. Liu, Q., Y. Gao, and B. Xu, *Liquid evaporation-driven folding of graphene sheets*. Applied Physics Letters, 2016. **108**(14): p. 141906.

APPENDICES

Appendix A

Appendix A.1

Table 1 Surface tension values matching each IPA ratio

	IPA	Density	Δh	r (Radius)	σ(ST)
1	0%	0.997	5.85	0.025	71.52
2	5%	0.9861	3.9	0.025	47.15
3	10%	0.976	3.1	0.025	37.1
4	15%	0.9654	2.9	0.025	34.33
5	20%	0.9507	2.8	0.025	32.6
6	25%	0.9445	2.5	0.025	29
7	30%	0.9339	2.3	0.025	26.34

Table. 1. shows the surface tension values march each IPA ratio.

Appendix A.2

Capillary method to measure the surface tension: calculations

We refer to the equation $\sigma = \frac{r g \Delta h \rho}{2}$ (1)

since we considered the contact angle $\theta = 0$

The density of water is given $\rho_{water} = 0.997 \text{ g/cm}^3$

Water will rise in a capillary tube with radius 0.025 to length 5.8 cm

$$\sigma_{water} = \frac{0.025 \times 981 \times 5.8 \times 0.997}{2} = 71 \text{ dyne/cm}$$

The density of IPA $\rho_{IPA} = 0.786 \text{ g/cm}^3$

IPA rises in a capillary tube with radius 0.025 is 2.4

$$\sigma_{IPA} = \frac{0.025 \times 981 \times 2.4 \times 0.786}{2} = 23.13 \text{ dyne/cm}$$

To calculate the surface tension of IPA+DI Water mixture, we need to calculate the density in each case:

$$\frac{1}{\rho} = \frac{X_{IPA}}{\rho_{IPA}} + \frac{X_{H2O}}{\rho_{H2O}} \quad (2)$$

X_{IPA} is the mass fraction of IPA

X_{H2O} is the mass fraction of water

*5% of IPA to 95% DI-Water

IPA =1.5 ml

DI Water =28.5 ml

The density of the above mixture is 0.9861 g/cm³

*10% of IPA to 90% DI-Water

IPA =3 ml

DI Water =20 ml

The density of the above mixture is 0.9760 g/cm³

*15% of IPA to 90% DI-Water

IPA =4.5 ml

DI Water =25.5 ml

The density of the above mixture is 0.9654 g/cm³

*20% of IPA to 80% DI-Water

IPA =6 ml

DI Water =24 ml

The density of the above mixture is 0.9507 g/cm³

*25% of IPA to 80% DI-Water

IPA =7.5 ml

DI Water =22.5 ml

The density of the above mixture is 0.9445 g/cm³

*30% of IPA to 70% DI-Water

IPA =9 ml

DI Water =21 ml

The density of the above mixture is 0.9339 g/cm^3

Using the equation (1) and the values of densities that we have got using eq.2:

1-For IPA= 5%

$r=0.025 \text{ cm}$

$\Delta h = 3.9 \text{ cm}$

$\rho = 0.9861 \text{ g/cm}^3$

$$\sigma_{IPA=5\%} = \frac{0.025 \times 981 \times 3.9 \times 0.9861}{2} = 47.15 \text{ dyne/cm}$$

2-For IPA= 10%

$r=0.025 \text{ cm}$

$\Delta h = 3.1 \text{ cm}$

$\rho = 0.97860 \text{ g/cm}^3$

$$\sigma_{IPA=10\%} = \frac{0.025 \times 981 \times 3.1 \times 0.97860}{2} = 37.10 \text{ dyne/cm}$$

3-For IPA 15%

$r=0.025 \text{ cm}$

$\Delta h = 2.9$

$\rho = 0.9654 \text{ g/cm}^3$

$$\sigma_{IPA=15\%} = \frac{0.025 \times 981 \times 2.9 \times 0.9654}{2} = 34.33 \text{ dyne/cm}$$

4-For IPA= 20%

$r=0.025 \text{ cm}$

$$\Delta h = 2.8 \text{ cm}$$

$$\rho = 0.9507 \text{ g/cm}^3$$

$$\sigma_{IPA=20\%} = \frac{0.025 \times 981 \times 2.8 \times 0.950}{2} = 32.60 \text{ dyne/cm}$$

5-For IPA= 25%

$$r=0.025 \text{ cm}$$

$$\Delta h = 2.5 \text{ cm}$$

$$\rho = 0.9445 \text{ g/cm}^3$$

$$\sigma_{IPA=25\%} = \frac{0.025 \times 981 \times 2.5 \times 0.9445}{2} = 29 \text{ dyne/cm}$$

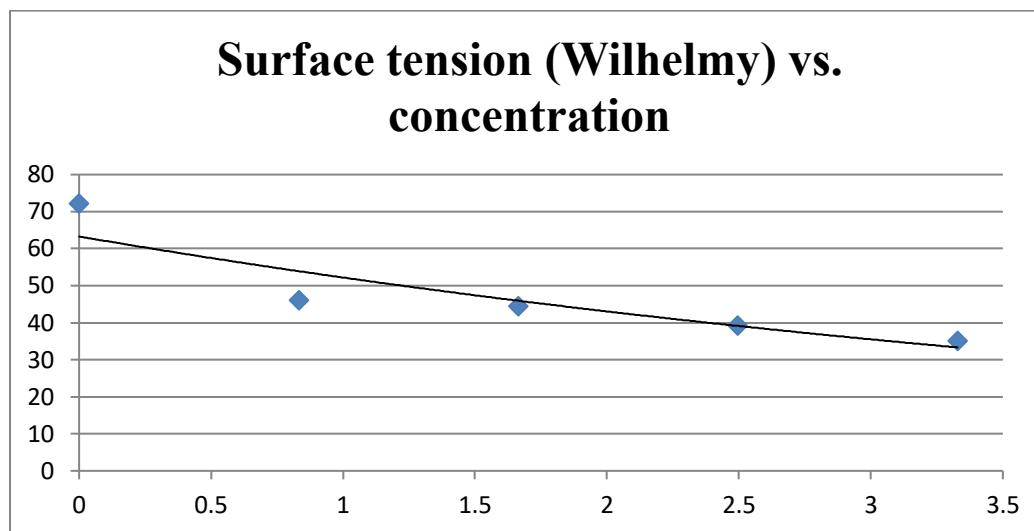
6-For IPA= 30%

$$r=0.025 \text{ cm}$$

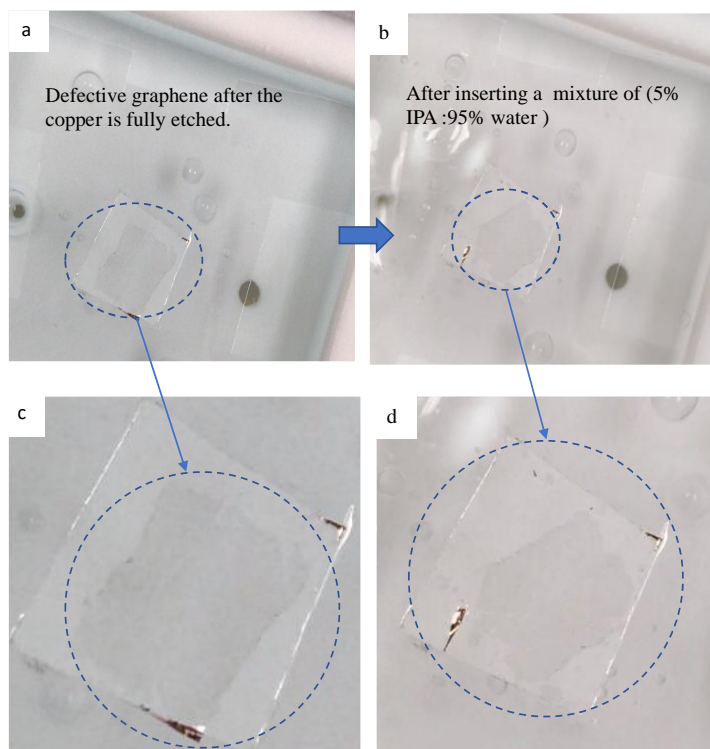
$$\Delta h = 2.3 \text{ cm}$$

$$\rho = 0.9339 \text{ g/cm}^3$$

$$\sigma_{IPA=30\%} = \frac{0.025 \times 981 \times 2.3 \times 0.9339}{2} = 26.34 \text{ dyne/cm}$$

Appendix A.3

Appendix A.4



a) Shows an image of defective graphene before applying STG. b) Shows the same graphene piece after applying 25 dyne/cm STG .c) Magnified image of the defective graphene shows visible cracks and edges deformation after the copper is fully etched. d) Magnified image shows the impact of applying 25 dyne/cm STG on defective graphene.

Appendix B

Appendix B.1

Hydrogel substrates preparation were prepared by mixing 1 g of agar powder and 0.2 g of gelatin sheets in 100 ml of boiling DI water. The mix was poured later in a plastic mold and left to solidify for 20 minutes.

FET device Fabrication. We fabricated shadow masks by following photolithography methods. Later, we used the electrodes shaped mask to deposit Cr 5 nm/Au 45 nm using a thermal vapor deposition system (thermal evaporator EDWARDS Auto 306). All the FET devices were annealed after fabrication at 300° C for one hour under vacuum. Finally, we shaped transfer graphene to narrow channels (width =1 mm) using radiofrequency argon plasma and the strips' shadow masks.

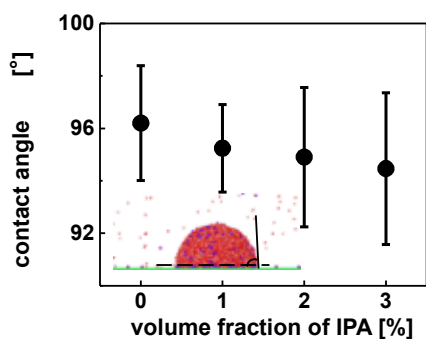
Characterization. Raman study on suspended and on-substrated garpahene was preforemd with 785 nm and 514.4 nm exciations, respectively. We performed AFM scanning of graphene on the Veeco MultiMode AFM system under tapping mode. The measurements of electron mobility on graphene FET devices were done on a homebuilt probe station combined with a source meter unit (SMU, Keithley 2450). SEM was performed on a Zeiss Merlin FE-SEM system, and the STEM imaging was captured at room temperature using a Nion UltraSTEM U100 microscope operated at 60 kV.

Appendix B.2

Statistics analysis. All graphene layers employed in this study has a size about 7 mm × 7 mm, and the GWM has a size of 1 cm × 1cm. The graphene roughness RMS of the three types of the transfer was measured from Veeco AFM Nanoscope software.

MD simulations. All MD simulations were carried out by the Large-scale Atomic/Molecular Massively Parallel Simulator (LAMMPS) package. [84] Graphene with a width of 4nm and a length of 10 nm was placed on the surface of the liquid mixture of water and IPA with 42000 water molecules. The simulation box size for peeling was 9.947 nm × 20.4192 nm × 20.0 nm, and the adaptive intermolecular reactive bond order (AIREBO) modeled flexible graphene. The SPC/E and TraPPE-UA potential models[85-88] were adopted for water and IPA molecules, respectively. For the nonbonded interactions, the 12–6 pairwise Lennard-Jones potential $V(r) = 4\epsilon(\sigma^{12}/r^{12} - \sigma^{12}/r^{12})$ and Coulomb interaction $V_q(r) = q_i q_j / 4\pi\epsilon_0 r$ were applied where r is the interatomic distance. At the same time, σ and ϵ are the equilibrium distance and the interactive well depth of the potential, respectively, q_i and q_j are the electronic charge counterpart, and ϵ_0 is the permittivity of the vacuum. Specifically, the Lennard-Jones parameters for graphite-water interaction were $\sigma_{CO} = 3.19 \text{ \AA}$ and $\epsilon_{CO} = 0.00407 \text{ eV}$.^[89, 90] The cut-off distance was 1 nm in this study. The Lorentz-Berthelot mixing rule was used to determine the inter-L-J parameters for different components. The particle–particle–particle–mesh (PPPM) algorithm with a root mean of 0.0001 was used to minimize the error of long-range Coulombic interactions. All simulations were run in an NVT ensemble with a Nose/Hoover thermostat set at 300 K unless otherwise stated.

Appendix B.3



The contact angle of the IPA-water mixture on graphene was calculated by MD simulations. Error bars indicate standard deviation during the NVE production period.